Non-Markovian delay-assisted sensing with waveguide-coupled quantum emitters

Prajit Dhara,[1,2,3,*] Isack Padilla,[1,†] Saikat Guha,[1,3,‡] Annyun Das,[1,4,§] and Kanu Sinha[1,4,‖]

[1]*Wyant College of Optical Sciences, The University of Arizona, Tucson, Arizona 85721, USA*

[2]*Quantum, Photonics, and Computing Group, RTX BBN Technologies, Cambridge, Massachusetts 02138, USA*

[3]*Department of Electrical and Computer Engineering, University of Maryland, College Park, Maryland 20742, USA*

[4]*Department of Physics, The University of Arizona, Tucson, Arizona 85721, USA*

(Received 21 May 2026; accepted 23 October 2026; published 6 November 2026)

We show that in a minimal setup of two waveguide-coupled quantum emitters, separated by long distances and subject to an external field, time-delayed feedback can be a resource for sensing field gradients. While the field gradient induces a detuning between the emitters, the large interatomic separations render the system dynamics non-Markovian. We show that the quantum Fisher information for estimating the detuning parameter, and thereby the field gradient, is enhanced in the presence of non-Markovian delay. Such an enhancement can be attributed to the formation of atom-photon quasibound states that enable the field to interact with the emitters for longer times, thereby gaining more information about their relative detunings. Additionally, in the presence of delay, the interaction between the emitters is mediated via multiple spectral modes of the field, further enhancing the sensing capabilities of the system. Our results establish non-Markovian time-delayed feedback and multimode reservoirs as a resource for distributed quantum sensing with waveguide-coupled quantum emitters.

DOI: 10.1103/m9nn-cgww

I. INTRODUCTION

Collections of quantum emitters coupled to waveguides are integral to physical implementations of distributed quantum information protocols [1–10]. In such waveguide quantum electrodynamics (QED) systems, as the characteristic delay between quantum emitters becomes comparable to the coherence length of a spontaneously emitted photon ($d \sim v/\gamma$), the memory effects of the field environment predominate the system dynamics (see Fig. 1). Waveguide-coupled emitters in presence of delay exhibit rich non-Markovian collective dynamics with instantaneous collective spontaneous emission rates exceeding those of regular superradiance [11–13], formation of atom-photon bound states in the continuum (BICs) [14–20], and multimode spectral effects [21–25]. In quantum information protocols with significant delays between emitters, time-delayed feedback is not only an essential element of consideration, but it can act as a resource, e.g., for generation of entangled atomic and photonic states [26–30], single-photon sources with improved coherence and indistinguishability [31], and quantum control via coherent time-delayed feedback [32].

Given that a structured, non-Markovian environment can enhance coherence by enabling information backflow, one can ask [33,34]: Can the memory effects of a non-Markovian field environment serve as a resource for sensing in waveguide QED systems? Furthermore, from a metrological perspective, for emitter separations comparable to or larger than the coherence length ($d \gtrsim v/\gamma$), the photonic environment acts as a multimode reservoir with an effective number of modes that scales as $\sim \gamma d/v$ [21,24]. This further motivates the question: Is it possible to leverage the multiple field environment modes as probes to enhance the sensitivity of parameter estimation?

In this work, we show that non-Markovian time-delayed interactions between waveguide-coupled emitters can assist in distributed quantum sensing of field gradients. We consider a minimal setup of two quantum emitters coupled to a one-dimensional waveguide, subject to an external field gradient, which induces a detuning between the emitters. We show that in such a system, non-Markovian delay is instrumental in enhancing the quantum Fisher information (QFI) [35] for estimating the field detuning, thereby improving measurement sensitivity. The resulting QFI, in general, is several orders of magnitude higher than that achieved by noninteracting emitters.

We further show that the enhancement in sensitivity, which occurs for specific values of detunings and delays, coincides with the formation of quasibound states of the atoms and photons in the "cavity" formed by the emitters. Such quasibound states in the continuum (qBICs) increase the effective memory of the field environment, or equivalently, the number of field modes participating in the collective system dynamics, which translates to the aforementioned sensitivity enhancements. The sensing advantages afforded by our approach are distinct from, and supplementary to the collective enhancements to sensitivity, using an ensemble of quantum systems [36–44].

*Contact author: prajit.dhara@rtx.com
†Contact author: iacpad0795@arizona.edu
‡Contact author: saikat@umd.edu
§Contact author: annyun@arizona.edu
‖Contact author: kanu@arizona.edu

Published by the American Physical Society under the terms of the Creative Commons Attribution 4.0 International license. Further distribution of this work must maintain attribution to the author(s) and the published article's title, journal citation, and DOI.

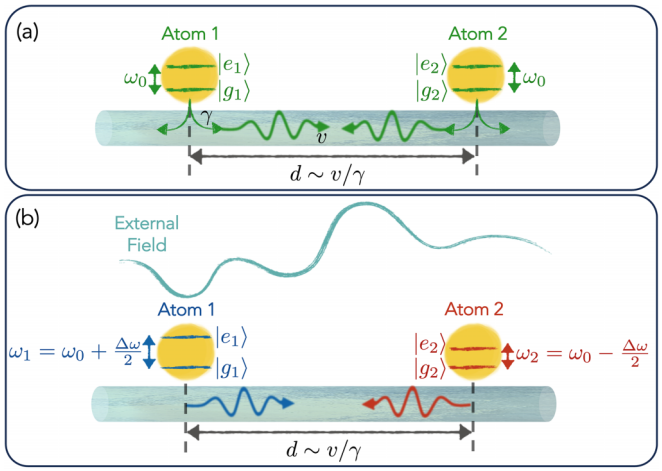


FIG. 1. (a) Two resonant two-level atoms coupled to a waveguide, with their mutual separation d comparable to the coherence length of a spontaneously emitted photon $d \sim v/\gamma$, where v is the speed of the electromagnetic field in the waveguide and γ is the spontaneous emission rate of an individual atom into the waveguide. (b) A spatially varying external field gradient creates a detuning between the emitters, with resulting resonant frequencies $\omega_1 = \omega_0 + \frac{\Delta\omega}{2}$ and $\omega_2 = \omega_0 - \frac{\Delta\omega}{2}$ for the emitters located at positions $x_1 = -d/2$ and $x_2 = d/2$ along the waveguide, respectively.

Our results provide the first example of environment-assisted sensing in waveguide QED systems, which form the basis for long-distance quantum information protocols.

The rest of the paper is organized as follows. In Sec. II, we present the model of two spatially separated emitters coupled via a waveguide and subject to an external field gradient that induces a detuning between the atomic resonances. We solve for the atomic dynamics, parametrized by the propagation delay and atomic detuning in Sec. III. In Sec. IV, we analyze the spectrum of the radiated field, identifying the specific parameter values (e.g., propagation delay and detuning) that correspond to an alignment. In Sec. V, we study the QFI associated with estimating the relative atomic detuning, identifying specific parameters for which there is an enhancement in sensing. We connect the QFI to the formation of atom-photon quasibound states in Sec. V B and provide a benchmark case with noninteracting atoms in Sec. V C. We present our conclusions and outlook in Sec. VI.

II. MODEL

The centerpiece of our analysis is a system comprising a pair of two-level emitters coupled via a one-dimensional waveguide and interacting with an external field whose gradient we aim to sense (see Fig. 1). The interaction between the external field and the individual emitters shifts their individual resonance frequencies $\omega_0 \to \omega_{1,2}$, such that $\omega_1 - \omega_2 = \Delta\omega$. The total Hamiltonian for the joint system may be expressed as $\hat{H} = \hat{H}_E + \hat{H}_F + \hat{H}_{\rm int}$. Here,

$$\hat{H}_E = \sum_{m=1,2} \hbar\omega_m \hat{\sigma}_+^{(m)} \hat{\sigma}_-^{(m)} \tag{1}$$

is the free Hamiltonian for the emitters with ω_m as the resonance frequency and $\hat{\sigma}_+^{(m)} = |e_m\rangle\langle g_m| = (\hat{\sigma}_-^{(m)})^\dagger$ as the atomic raising operator of the mth emitter. The free Hamiltonian for the waveguide modes is

$$\hat{H}_F = \int_0^\infty {\rm d}k\, \hbar\omega [\hat{a}_R^\dagger(k)\hat{a}_R(k) + \hat{a}_L^\dagger(k)\hat{a}_L(k)], \tag{2}$$

where $\hat{a}_R^\dagger(k)$ and $\hat{a}_L^\dagger(k)$ are the bosonic creation (annihilation) operators for the right- and left-propagating field modes of the waveguide, respectively, and satisfy the canonical commutation relations $[\hat{a}_R(k), \hat{a}_R^\dagger(k')] = [\hat{a}_L(k), \hat{a}_L^\dagger(k')] = \delta(k-k')$. We assume the waveguide to have a linear dispersion such that $k = \omega/v$. The interaction between the emitters and the waveguide modes is described by $\hat{H}_{\rm int}$, which, upon making the electric-dipole and rotating-wave approximations, can be expressed in the interaction picture as

$$\hat{H}_{\rm int} = \hbar \sum_{m=1,2} \int_0^\infty {\rm d}\omega\, g(\omega)\hat{\sigma}_+^{(m)} [\hat{a}_R(\omega) e^{i\omega x_m/v} + \hat{a}_L(\omega) e^{-i\omega x_m/v}] e^{-i(\omega-\omega_m)t} + {\rm H.c.} \tag{3}$$

Here, $g(\omega)$ is the atom-field coupling strength; we assume a flat-spectral density around the resonant frequencies of the emitters such that $g(\omega) \approx g(\omega_0)$. The two emitters are located at $x_1 = -d/2$ and $x_2 = d/2$ along the waveguide axis, such that the interatomic separation d can be large and comparable to the coherence length $\sim v/\gamma$ associated with a spontaneously emitted photon. The detuning between the atoms ($\Delta\omega$) could arise from a multitude of external factors, including but not limited to magnetic, electric, thermal, and strain fields. The generic form of the interaction is $\hat{H}_{\rm ext} = \boldsymbol{\mu} \cdot \boldsymbol{\Delta F}\, \hat{\sigma}_+^{(m)} \hat{\sigma}_-^{(m)}$, where $\boldsymbol{\mu}$ is a generic susceptibility and $\boldsymbol{\Delta F}$ is the vector-valued field gradient.

We assume that the initial state of the total system is $|e_1, g_2\rangle|\{0\}\rangle$, wherein emitter 1 is prepared in an excited state while emitter 2 is in the ground state; $|\{0\}\rangle$ denotes the vacuum state for the waveguide modes. We remark that the system is initialized in an unentangled state, wherein we are not leveraging entanglement as a metrological resource to start with [45]. Since the total Hamiltonian preserves the total number of excitations in the atomic + field Hilbert spaces, the system remains in a single-excitation manifold at all times. The joint emitters-field state at any time $t \geqslant 0$ is thus

$$|\Psi_{\eta,\delta}(t)\rangle = \sum_{m=1,2} c_m(t)\hat{\sigma}_+^{(m)}|g_1, g_2, \{0\}\rangle + \int_0^\infty {\rm d}\omega \times [c_R(\omega, t)\hat{a}_R^\dagger(\omega) + c_L(\omega, t)b^\dagger(\omega)]|g_1, g_2, \{0\}\rangle, \tag{4}$$

where $c_m(t)$ represents the excitation amplitude for the mth emitter, and $c_R(\omega, t)$, $c_L(\omega, t)$ are the field excitation amplitudes for the right- and left-going waveguide modes, respectively. Here, we have parametrized the quantum state of the total system with dimensionless distance $\eta \equiv \gamma d/v$ and detuning $\delta \equiv \Delta\omega/\gamma$. We now consider the dynamics of the total detuned emitters + field system under the Hamiltonian [Eq. (3)] in the single-excitation subspace.

III. COLLECTIVE DYNAMICS OF DETUNED EMITTERS

We first trace over the field modes, including the self-consistent backaction of the field on the emitters, to determine

the coupled dynamics of the two detuned atoms as follows (see Appendix A for details):

$$\dot{c}_1(t) = -\frac{\gamma}{2}\left[c_1(t) + \beta c_2\left(t-\frac{d}{v}\right)\Theta\left(t-\frac{d}{v}\right)e^{i\omega_2 d/v + i\Delta\omega t}\right], \tag{5}$$

$$\dot{c}_2(t) = -\frac{\gamma}{2}\left[c_2(t) + \beta c_1\left(t-\frac{d}{v}\right)\Theta\left(t-\frac{d}{v}\right)e^{i\omega_1 d/v - i\Delta\omega t}\right], \tag{6}$$

where $\gamma = 2\pi|g(\omega_0)|^2$ and β represents the coupling efficiency of the emitters to the waveguide, which we will assume to be $\beta = 1$, unless stated otherwise. The first term in the above equations corresponds to spontaneous decay of each emitter; the second term represents the waveguide-mediated time-delayed feedback of one emitter on the other while accounting for the appropriate propagation phase ($e^{i\omega_m d/v}$) and the detuning between the emitters ($e^{i\Delta\omega t}$). The solution to the coupled atomic dynamics in Eqs. (5) and (6) involves inversion of the Laplace-transformed coefficients, $\mathcal{C}_m(s) = \int_0^\infty \mathrm{d}t\, c_m(t)e^{-st}$:

$$\gamma\mathcal{C}_1(s) = \frac{(\tilde{s} - i\delta + 1/2)}{(\tilde{s}+1/2)(\tilde{s}-i\delta+1/2) - \beta^2(e^{i\phi_1}e^{-\eta\tilde{s}}/2)^2}, \tag{7}$$

$$\gamma\mathcal{C}_2(s) = \frac{-\beta e^{i\phi_2}e^{-\eta\tilde{s}}/2}{(\tilde{s}+1/2)(\tilde{s}+i\delta+1/2) - \beta^2(e^{i\phi_2}e^{-\eta\tilde{s}}/2)^2}, \tag{8}$$

where we use the normalized variable, $\tilde{s} \equiv s/\gamma$, and the propagation phase associated with each frequency is $\phi_m = \omega_m d/v$. We note that the propagation phases $\phi_{\{1,2\}}$ must satisfy the self-consistent relation

$$\phi_1 - \phi_2 = \frac{(\omega_1 - \omega_2)d}{v} = \delta\eta. \tag{9}$$

We now analyze the emitter dynamics resulting from the inverse Laplace transform of Eqs. (7) and (8) that can be expressed in two different forms: (1) a series solution [46,47] that illustrates the time-delayed feedback on the atomic dynamics from the field environment; or (2) a multiexponential decay [11] that illustrates the multimode nature of the field environment in the presence of retardation, as we will discuss further below.

A. Series solution

The atomic dynamics can be written in terms of a series solution as follows (see Appendix A 1 for details):

$$c_1(t) = e^{-\gamma t/2} + e^{i\delta\gamma t/2}\sum_{n=1}^{\infty}\Xi_n^{(1)}(t)\beta^{2n}e^{in(\phi_1+\phi_2)} \times e^{-(\gamma t - 2n\eta)/2}\Theta(\gamma t - 2n\eta), \tag{10}$$

$$c_2(t) = e^{-i\delta\gamma t/2}\sum_{n=0}^{\infty}\Xi_n^{(2)}(t)\beta^{2n+1}e^{i(2n+1)(\phi_1+\phi_2)/2} \times e^{-(\gamma t-(2n+1)\eta)/2}\Theta[\gamma t - (2n+1)\eta]. \tag{11}$$

Each term in the above series corresponds to the modification of atomic dynamics after a round trip of the field between the emitters, as seen from the Heaviside theta functions $\{\Theta(\gamma t - 2n\eta),\ \Theta(\gamma t - (2n+1)\eta)\}$, which make the non-Markovian time-delayed feedback manifest (as shown in Fig. 2). The first term in the atom 1 dynamics $c_1(t)$ corresponds to its independent decay and the second term to the time-delayed feedback from atom 2 at every $t = 2nd/v$ that incorporates the waveguide coupling efficiency ($\sim\beta^{2n}$) and the round-trip propagation phase $e^{in(\phi_1+\phi_2)}$. Similarly, the excitation dynamics of atom 2 results exclusively due to the time-delayed feedback from atom 1 at every $t = (2n+1)d/v$. The dynamics of atom 1 (2), as "driven" by atom 2 (1), exhibits oscillations with frequencies $\Delta\omega/2 = \delta\gamma/2$ ($-\Delta\omega/2 = -\delta\gamma/2$) [48]. The terms $\Xi_n^{(m)}(t)$ correspond to the nonexponential part of the atomic dynamics; their explicit expressions are given in Appendix A 1.

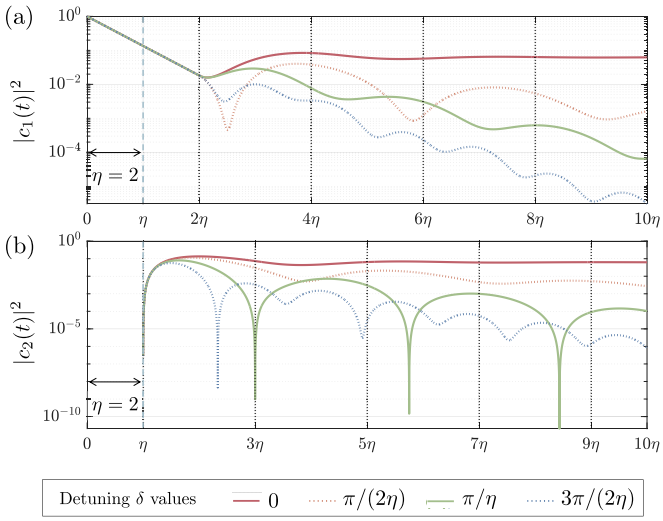


FIG. 2. Emitter dynamics in the presence of detuning for the initial state $|e\rangle_1|g\rangle_2|\{0\}\rangle$. Emitter excitation probabilities (log-scaled) for emitters 1 [panel (a)] and 2 [panel (b)] as a function of time (γt) and interatomic separation $\eta = 2$ for detuning values $\delta = \{0, \frac{\pi}{2\eta}, \frac{\pi}{\eta}, \frac{3\pi}{2\eta}\}$. The vertical gray dotted lines represent the time intervals for the field excitation round trip between the two emitters ($t = nd/v$ or $\gamma t = n\eta$).

B. Multiexponential decay

We invert $\mathcal{C}_i(s)$ based on Cauchy's residue theorem to obtain the atomic dynamics expressed as a multiexponential decay (see Appendix A 2 for details):

$$c_m(t) \equiv \sum_j R_j^{(m)} e^{\tilde{s}_j^{(m)}\gamma t}, \tag{12}$$

where $\tilde{s}_j^{(m)}$ and $R_j^{(m)}$ are the poles and residues corresponding to the inverse Laplace transform of $\mathcal{C}_m(s)$, evaluated semianalytically. For practical purposes, one may truncate the pole index summation to a finite cutoff value $|j| \leqslant j_{\mathrm{cut}}$; higher order poles capture larger frequencies with progressively smaller contributions [11].

The multiexponential decay form of the emitter dynamics alludes to a multimode field environment that mediates the interatomic interactions. Physically, this can be understood as follows: The "cavity" formed by the two emitters has a free

spectral range (FSR)

$$\Delta_{\mathrm{FSR}} \equiv \frac{\pi v}{d}; \tag{13}$$

thus, as $\eta \sim \gamma/\Delta_{\mathrm{FSR}} \gtrsim 1$, the atomic linewidth encompasses multiple such cavity modes [23–25]. As we will show, such multimode dynamics, mathematically equivalent to the non-Markovian time-delayed feedback, is crucial to enhancing the detuning sensitivity highlighted in Sec. V. In essence, we demonstrate that increasing the number of environment degrees of freedom participating in the system dynamics, or equivalently, extending the environment's memory time, can enhance the sensitivity for estimating system parameters.

C. Detuned emitter dynamics

The introduction of detuning modifies the collective emitter dynamics, as noted previously in Eqs. (10) and (11). We highlight this in Fig. 6, where we plot excitation probability dynamics $[|c_1(t)|^2, |c_2(t)|^2]$ for the two emitters as a function of time (γt) with a fixed separation $\eta = 2$, and different values of the detuning δ chosen as $\delta = n\pi/(2\eta)$ $(n \in \mathbb{Z}^+)$. We choose the propagation phase

$$\phi_2 = 2p\pi, \quad p \in \mathbb{Z}^+, \tag{14}$$

for the resonantly emitted field from emitter 2, such that $\omega_2 = 2p\Delta_{\mathrm{FSR}}$, which coincides with one of the geometric resonances of the cavity formed by the emitters. The corresponding propagation phase for the resonantly emitted field from atom 1 becomes

$$\phi_1 = 2p\pi + \delta\eta \Rightarrow \omega_1 = \left(2p + \frac{n}{2}\right)\Delta_{\mathrm{FSR}}. \tag{15}$$

Thus, for even values of n we have the resonance of atom 1 coincide with one of the *atomic cavity* resonances, while for odd values of n there is an offset between the resonance of emitter 1 and that of the atomic cavity. Figures 6(a) and 6(b) show that the dynamics of emitter 1 (2) is influenced by the time-delayed feedback from emitter 2 (1) every γt that is an even (odd) multiple of η, in agreement with Eqs. (10) and (11) (time intervals marked by gray vertical lines). For resonant emitters ($\delta = 0$, red solid line), the emitters have a finite excitation probability in the steady state. This can be understood as follows: The initial state of the emitters $|e_1, g_2\rangle$ is an equal superposition of a superradiant $(\frac{1}{\sqrt{2}}(|e_1, g_2\rangle + |g_1, e_2\rangle))$ and subradiant $(\frac{1}{\sqrt{2}}(|e_1, g_2\rangle - |g_1, e_2\rangle))$ state; while the symmetric superradiant part radiates into the field modes, the antisymmetric dark state forms an atom-photon bound state [11,14,16]. Detuning between emitters prevents the formation of a bound steady state. As a notable feature, the rate of change in atom 1 excitation probability as it "sees" a retarded backaction from atom 2, determined by the slope of $|c_1(t)|^2$ at $\gamma t = 2\eta$, is positive (negative) when the detuning δ is an even (odd) multiple of $\pi/(2\eta)$. Thus, for a fixed separation, the choice of detuning determines the revival of atomic excitation, and concomitantly the emission from the atoms into the field. We will see that detunings, δ, that are odd integer multiples of $\pi/(2\eta)$, lead to the formation of a quasibound state of emitters and the field in the "atomic cavity" region. In subsequent section, we examine the field spectrum, which supports this observation and, as we will show later in Sec. V, assists in field gradient sensing.

IV. FIELD SPECTRUM

We now analyze the spectrum of the field radiated by the atoms. Given the non-Markovian nature of the dynamics, the field environment plays a critical role in the collective dynamics of the atoms, and consequently in sensing the relative atomic detuning.

The field excitation amplitudes in the steady state $(t \to \infty)$ can be written as (see Appendix A)

$$c_R(\tilde{\omega}, \infty) = -i\sqrt{\frac{\gamma}{2\pi}}[e^{i\tilde{\omega}\eta/2}F_1(\tilde{\omega}) + e^{-i\tilde{\omega}\eta/2}F_2(\tilde{\omega})], \tag{16}$$

$$c_L(\tilde{\omega}, \infty) = -i\sqrt{\frac{\gamma}{2\pi}}[e^{-i\tilde{\omega}\eta/2}F_1(\tilde{\omega}) + e^{i\tilde{\omega}\eta/2}F_2(\tilde{\omega})], \tag{17}$$

where $\tilde{\omega} = \omega/\gamma$. The atomic frequency response functions, $F_1(\tilde{\omega})$ and $F_2(\tilde{\omega})$, are defined as the Fourier transforms of the atomic coefficients $F_m(\tilde{\omega}) = \int_0^\infty \mathrm{d}t\, c_m(t)e^{i(\tilde{\omega}-\tilde{\omega}_m)\gamma t}$, which describe the frequencies present in the atomic dynamics. We note from Eqs. (16) and (17) that the field excitation amplitudes $(c_{a,b}(\tilde{\omega}, \infty))$ result from the interference of the fields radiated by the two emitters, incorporating the propagation phase $(e^{\pm i\tilde{\omega}\eta/2})$ between the emitters. The response functions $F_m(\tilde{\omega})$ are given by (see Appendix B for details)

$$\gamma F_1(\tilde{\omega}) = \frac{-i[(\tilde{\omega} - \tilde{\omega}_0) + \delta/2] + 1/2}{D(\tilde{\omega})}, \tag{18}$$

$$\gamma F_2(\tilde{\omega}) = -\frac{e^{i\eta\tilde{\omega}}/2}{D(\tilde{\omega})}, \tag{19}$$

with the denominator $D(\tilde{\omega})$:

$$D(\tilde{\omega}) = \left[-i(\tilde{\omega} - \tilde{\omega}_0) + \frac{1}{2}\right]^2 + \frac{\delta^2}{4} - \frac{e^{2i\eta\tilde{\omega}}}{4}. \tag{20}$$

The roots of $D(\tilde{\omega})$ capture the characteristic frequencies present in the dynamics of the emitters. Appendix B shows that the peak frequencies in the dynamics of atom 1 are centered at $\tilde{\omega}_1$, and those for atom 2 are located symmetrically at $\tilde{\omega}_1$ and $\tilde{\omega}_2$ (see Fig. 7).

The steady-state spectrum of the emitted field can be defined as

$$G(\tilde{\omega}) \equiv |c_R(\tilde{\omega}, \infty)|^2 + |c_L(\tilde{\omega}, \infty)|^2, \tag{21}$$

which represents the probability of excitation of a field mode with frequency $\tilde{\omega}$. This can be expressed in terms of the atomic frequency responses as

$$G(\tilde{\omega}) = \frac{\gamma}{\pi}[|F_1(\tilde{\omega})|^2 + |F_2(\tilde{\omega})|^2 + 2\cos(\tilde{\omega}\eta)\mathrm{Re}[F_1^*(\tilde{\omega})F_2(\tilde{\omega})]]. \tag{22}$$

Figure 3 shows the emitted field spectrum $G(\tilde{\omega})$ as a function of frequency $\tilde{\omega}$ and the interatomic separation η, for three separate values of the detuning δ. We highlight the salient features of the field spectrum as follows:

(1) For resonant emitters ($\delta = 0$), the spectrum peaks are obtained via the zeros of the denominator of Eqs. (B3) and

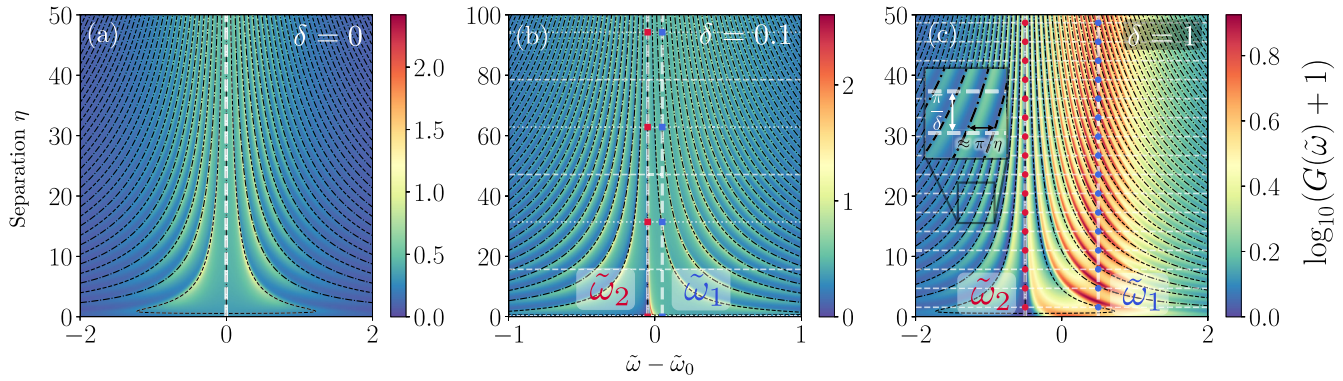


FIG. 3. Field spectrum $G(\tilde{\omega})$ as a function of the frequency $\tilde{\omega} - \tilde{\omega}_0$ and the interatomic separation η for different values of detuning: (a) $\delta = 0$, (b) $\delta = 0.1$, and (c) $\delta = 1$. The vertical dashed lines marked as $\tilde{\omega}_{1,2}$ indicate the resonances of the two emitters. The peaks of the spectrum obtained from Eq. (24) are denoted by the black dash-dotted ($\tilde{\omega}^{+}_{n\delta} - \tilde{\omega}_0$) and black dashed ($\tilde{\omega}^{-}_{n\delta} - \tilde{\omega}_0$) curves. The horizontal white dotted and dashed lines in panels (b) and (c) represent specific values of $\eta_n = n\pi/\delta$ and $\eta_{n+1/2} = (n + 1/2)\pi/\delta$, respectively. The blue (red) squares and circles indicate the intersections of the horizontal $\eta = \eta_n$ and $\eta = \eta_{n+1/2}$ lines with the atomic resonances $\tilde{\omega}_1 - \tilde{\omega}_0$ ($\tilde{\omega}_2 - \tilde{\omega}_0$), respectively. The highlighted inset region in panel (b) shows that the separation between the adjacent horizontal white η_n lines is π/δ for a fixed $\tilde{\omega}$ [Eq. (25)], while for a fixed (large) separation η the free spectral range between two adjacent spectral peaks is $\approx\pi/\eta$ [Eq. (27)], akin to a Fabry-Pérot cavity.

(B4) ($D(\tilde{\omega}^{\pm}_{n0}) = 0$) as follows [21]:

$$\tilde{\omega}^{\pm}_{n0} = \tilde{\omega}_0 + \frac{1}{\eta}\mathrm{Im}\Big[W_n\Big(\pm\frac{\eta}{2}e^{\eta/2}\Big)\Big], \quad n \in \mathbb{Z}, \tag{23}$$

where $W_n(\cdot)$ is the nth branch of the Lambert W function. We have assumed a propagation phase of $\phi_0 = \phi_1 = \phi_2 = 2p\pi$ ($p \in \mathbb{Z}^+$) for resonant emitters. Figure 3(a) shows the spectrum of the field emitted from two resonant emitters, where we note that the peaks of the emission coincide with the black dash-dotted and dashed curves representing $\tilde{\omega}^{+}_{n0} - \tilde{\omega}_0$ and $\tilde{\omega}^{-}_{n0} - \tilde{\omega}_0$, respectively.

(2) For detuned emitters, we observe from Fig. 3(b) ($\delta = 0.1$) and Fig. 3(c) ($\delta = 1$) that, as expected, the field emission from initially excited atom 1 is peaked at its resonance frequency $\tilde{\omega}_1$. For large η, the peaks of the emission spectrum can be approximated by

$$\tilde{\omega}^{\pm}_{n\delta} = \tilde{\omega}_0 - \frac{\delta}{2} + \frac{1}{\eta}\mathrm{Im}\Big[W_n\Big(\pm\frac{\eta}{2}e^{\eta/2}\Big)\Big], \quad n \in \mathbb{Z}, \tag{24}$$

as seen from the black dash-dotted and dashed curves in Figs. 3(b) and 3(c). The above expression reduces to Eq. (23) for $\delta = 0$.

(3) When the emitter 1 resonance ($\tilde{\omega}_1$) is coincident with the resonances of the atomic "cavity," such that $\tilde{\omega}_1 = \tilde{\omega}^{\pm}_{n\delta}$, we observe a stronger overall emission, as indicated by the blue squares and circles in Figs. 3(b) and 3(c), respectively. This occurs for specific values of the atomic separation $\{\eta_{n+1/2}, \eta_n\}$, depending on the relative atomic detuning δ (see Appendix B 2 for details):

$$\eta_{n+1/2}\delta \approx \big(n + \tfrac{1}{2}\big)\pi, \quad \text{for } \delta \gtrsim 1, \tag{25}$$

$$\eta_n\delta \approx n\pi, \quad \text{for } \delta \ll 1. \tag{26}$$

(4) The difference between the subsequent resonances of the emitted field spectrum, $|\tilde{\omega}^{+}_{n\delta} - \tilde{\omega}^{-}_{n\delta}|$, converges to (see Appendix B 2)

$$|\tilde{\omega}^{+}_{n\delta} - \tilde{\omega}^{-}_{n\delta}| \to \frac{\pi}{\eta} = \frac{\Delta_{\mathrm{FSR}}}{\gamma} \tag{27}$$

in the large η limit, recovering the FSR of a Fabry-Pérot cavity of length d [49].

We will see in the next section that the conditions $\eta_{n+1/2}\delta \approx (n + 1/2)\pi$ (for $\delta \gtrsim 1$) and $\eta_n\delta \approx n\pi$ (for $\delta \ll 1$), where there is an alignment of the atom 1 resonance with that of the "cavity" region between the atoms, there is a formation of atom-photon quasibound states. Thus, the excitation is kept for longer times in the form of field buildup inside the two-atom "cavity." We hypothesize that such quasibound states, which are quintessentially non-Markovian, can potentially enhance sensing, as we will now demonstrate.

V. SENSING EXTERNAL FIELDS

Having developed a framework to evaluate the quantum state of the emitters and the field environment, we now evaluate the QFI associated with sensing the relative atomic detuning δ. The QFI bounds the highest precision in estimating δ attainable by any measurement as per the quantum Cramér-Rao bound [50].

A. Quantum Fisher information

Throughout our analysis, we assume perfect emitter-waveguide coupling ($\beta = 1$), which implies that the state of the total atom + field system remains pure at a general time $t > 0$:

$$\rho_{\delta,\eta}(t) \equiv |\Psi_{\delta,\eta}(t)\rangle\langle\Psi_{\delta,\eta}(t)|. \tag{28}$$

For a pure state, the QFI, $H(\delta)$, can be simplified as [51]

$$\begin{aligned} H(\delta;t) &= 4\mathrm{Tr}\rho_{\delta,\eta}(t)\Big(\frac{\partial\rho_{\delta,\eta}(t)}{\partial\delta}\Big)^2 \\ &= 4[\mathrm{Re}\langle\partial_\delta\Psi_{\delta,\eta}(t)\,|\,\partial_\delta\Psi_{\delta,\eta}(t)\rangle \\ &\quad + \langle\Psi_{\delta,\eta}(t)\,|\,\partial_\delta\Psi_{\delta,\eta}(t)\rangle^2], \end{aligned} \tag{29}$$

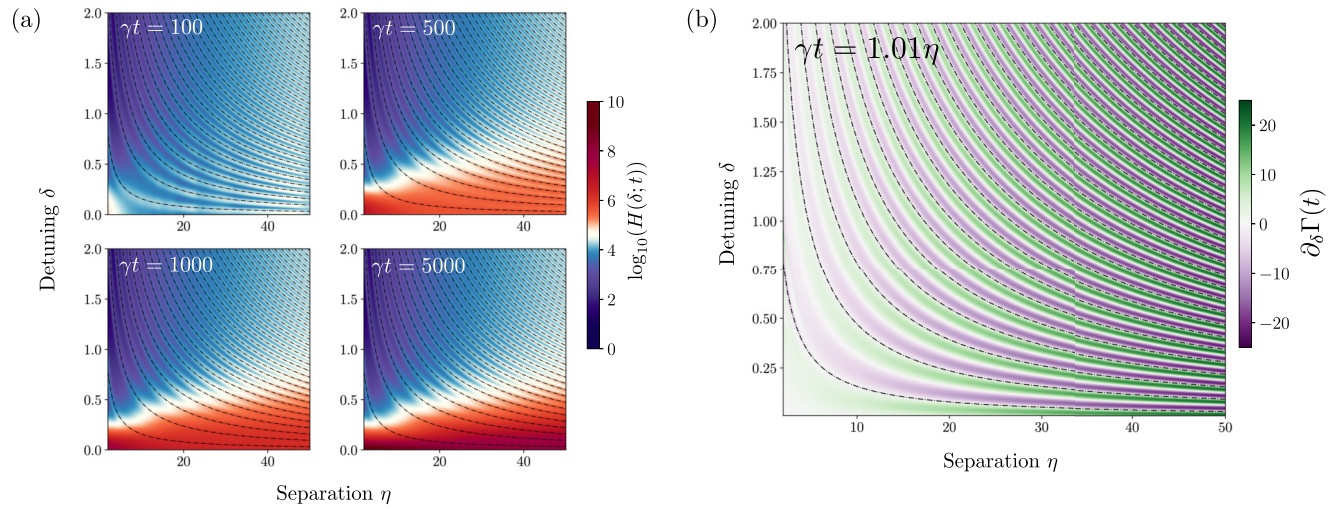


FIG. 4. Quantum Fisher information $[H(\delta;t)]$ and quasibound-state decay rate derivative $[\partial_\delta \Gamma_{\mathrm{qBIC}}(t)]$ for initial state $|e,g\rangle$ for varying atomic detuning (δ) and separation (η). (a) QFI of the system with respect to δ evaluated at four times $\gamma t = 100, 500, 1000, 5000$, where steady state has been reached in the bottom right panel. (b) Derivative of the quasibound-state excitation decay with respect to δ, at a separation-dependent time $\gamma t \to \eta^+$, right after the field from emitter 1 reaches emitter 2. For each quantity, we note that the hyperbolae of constant propagation phase $\delta\eta = (n + 1/2)\pi$; $n \in \mathbb{Z}^+$ (black dot-dashed lines) are local maxima.

where $|\partial_\delta \Psi_{\delta,\eta}(t)\rangle$ is the covariant derivative of $|\Psi_{\delta,\eta}(t)\rangle$ with respect to δ on the manifold of pure states [52]. A detailed derivation of the QFI is provided in Appendix C.

Figure 4(a) shows the QFI $H(\delta;t)$ as a function of interatomic separations (η) and detunings (δ) at various points in time (marked by the inset label), which is the central result of this work. We highlight below the key features of Fig. 4(a), which can be broadly understood from the buildup of field excitations inside the "cavity" formed by the two atoms, resulting in a longer interaction time over which the field interacts with the atoms before leaking out:

(1) We note that the QFI generally increases with time, attaining a steady-state value as $t \to \infty$. This can be attributed to the longer time of interaction between the emitters and the field that probes their relative detuning.

(2) At a fixed time snapshot and for a fixed atomic separation η, the QFI generally decreases with increasing the detuning δ. The relative atomic detuning δ affects the "cavity loss rate." Thus, for small δ the intracavity field decays slowly, allowing for longer interaction time between the field and the emitters, and consequently, improved sensitivity of their relative detuning.

(3) For a fixed δ, we identify two distinct trends for the QFI with varying atomic separation η. First, for small detunings (e.g., $\delta \lesssim 0.2$ region), we observe that the QFI generally decreases with the separation η. This can be understood as follows: For small detunings and small distances, the two emitters form a near-perfect bound state, which generally enhances the QFI. However, with increasing the interatomic separation, some field leaks out of the "atomic cavity" before a quasibound state is formed.

(4) For larger detuning values ($\delta \gtrsim 1$), e.g., when the emitter resonances are separated by a linewidth or more, the multimode nature of the dynamics for large η starts to become significant. Particularly, we note that the QFI is maximum along hyperbolic curves of the η-δ plane. Specifically, these correspond to hyperbolae

$$\eta\delta = \left(n + \tfrac{1}{2}\right)\pi, \quad n \in \mathbb{Z}^+, \tag{30}$$

which is precisely the condition where resonance of emitter 1 aligns with the resonances of the "atomic cavity" [Eq. (25)]. Such an alignment of atomic resonances with those of the "cavity" leads to a resonant buildup of field, allowing the field to probe atoms for longer before it leaks. We will substantiate this observation by analyzing the formation of quasibound states in the next section.

(5) Figure 5 shows the QFI for small detunings $\delta \leqslant 0.2$. We plot the QFI $H(\delta;t)$ as a function of the separation (η) along the hyperbolae $\eta\delta = \alpha$, where $\alpha = \{n\pi, (n + \frac{1}{2}\pi)\}$, for $\gamma t = 10^5$. We note that the QFI for $\alpha = n\pi$ (dashed lines) is consistently higher than that of $\alpha = (n + 1/2)\pi$ (dash-dotted lines) for the same $n \in \mathbb{N}$. This is also evident from the contour plot of $H(\delta;t)$ in Fig. 5(b), where the local maxima shift to

$$\eta\delta = n\pi, \tag{31}$$

consistent with Eq. (26), such that the detuned emitter frequency aligns with the effective cavity resonances. The slower intracavity field decay in the small detuning regime is the primary reason the shift in the QFI maxima occurs at large times.

B. Quasibound-state formation

As discussed in Secs. III and IV, the collective dynamics of two waveguide-coupled resonant emitters separated by a long distance can result in a delocalized atom-photon bound state, arising from the destructive interference between the atoms and the fields propagating between them [11,14,16]. However, as noted previously, perfect BICs cannot emerge with finite detuning ($\delta \neq 0$) since the destructive interference between the fields emitted by each atom is no longer perfect, owing to

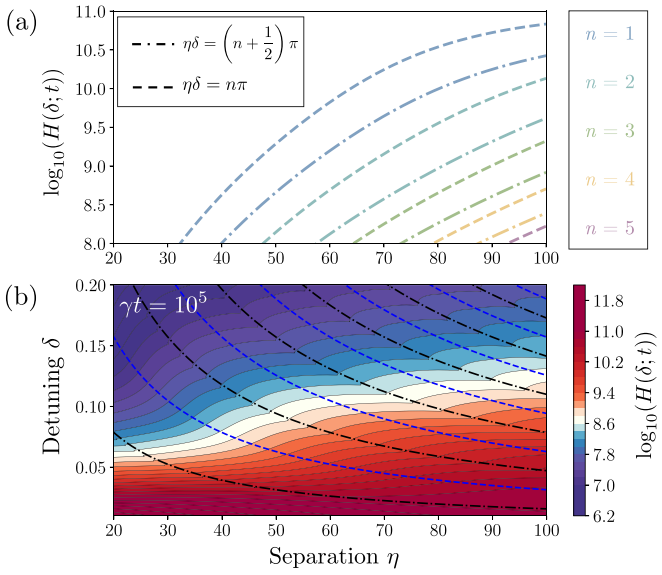


FIG. 5. Quantum Fisher information $H(\delta;t)$ for small detunings ($\delta \lesssim 0.2$) at long times ($\gamma t = 10^5$). (a) QFI along $\eta\delta = (n + 1/2)\pi$ (dot-dashed lines) and $\eta\delta = n\pi$ (dashed lines) hyperbolae. (b) QFI contour plot. For small detunings, the local maxima condition for QFI is at $\eta\delta = n\pi$, consistent with Eq. (26).

their resonant frequency mismatch. While one can not have perfect bound states for two detuned emitters, the system still supports long-lived quasibound states of the atoms and the field, which enable an enhancement in the resulting QFI.

To analyze such quasibound states, we consider the total probability of the single excitation being in either of the two atoms, or in the waveguide field modes occupying the region between the two atoms ($x \in [-d/2, d/2]$) [53]:

$$P_q(t) = \sum_{m=1,2} |c_m(t)|^2 + \int_{-d/2}^{d/2} \mathrm{d}x\, [|c_R(x,t)|^2 + |c_L(x,t)|^2], \tag{32}$$

where

$$c_R(x,t) = \frac{1}{2\pi}\int_0^\infty \mathrm{d}\omega\, c_R(\omega,t) e^{-i\omega(t-x/v)}$$
$$c_L(x,t) = \frac{1}{2\pi}\int_0^\infty \mathrm{d}\omega\, c_L(\omega,t) e^{-i\omega(t+x/v)}, \tag{33}$$

are the Fourier transforms of $c_R(\omega,t)$ and $c_L(\omega,t)$, respectively, switched from the frequency domain to spatial domain.

The time derivative of Eq. (32) gives us the excitation decay rate [53] from the two-atom + cavity region:

$$\Gamma(t) \equiv \frac{\mathrm{d}P_q(t)}{\mathrm{d}t}. \tag{34}$$

The values of η and δ that minimize $\Gamma(t)$ correspond to a suppressed field leakage from the effective cavity formed by the two atoms, indicating the formation of a quasibound state of the emitters and photons. In such a qBIC, the extended atom-field interaction time enables the field modes to interrogate the emitters for longer, and consequently carry more information about the relative atomic detuning once they leak.

We distinguish between two time regimes: before and after the initially emitted radiation of emitter 1 reaches emitter 2. Since we are interested in the late-time QFI, the decay rate for $t > d/v$ is given as

$$\Gamma\left(t > \frac{d}{v}\right) = \sum_{m=1,2}\left[\frac{\gamma}{8\pi}\left\{|c_m(t)|^2 - \left|c_m\left(t - \frac{d}{v}\right)\right|^2\right\} + \frac{\mathrm{d}}{\mathrm{d}t}|c_m(t)|^2\right], \tag{35}$$

where the $(|c_m(t)|^2 - |c_m(t - d/v)|^2)$ term corresponds to the total transfer of excitation probability from the emitters to the field in one round trip and $d|c_m(t)|^2/dt$ represents the instantaneous rate of excitation for the individual emitters. Taken together, these two contributions capture the decay rate of the total excitation in the emitters and the field that occupies the cavity region.

In Fig. 4(b), we plot the gradient of the qBIC loss rate $\partial_\delta \Gamma(t \to (d/v)^+)$ for each point in the η-δ plane. We observe that the relation between η and δ for which there exists a qBIC:

$$\eta\delta = \left(n + \tfrac{1}{2}\right)\pi \tag{36}$$

matches the one for maximal QFI [Eq. (30)], as well as the condition for the atomic resonances to align with those of the "cavity" [Eq. (25)]. Thus, as pointed earlier in Sec. IV, the alignment between the emitter resonances with those of the cavity boosts the emission from the atoms into the field, as well as supports the formation of a qBIC that enhances field buildup, prolonging atom-field interaction and thereby the QFI. The details of the calculation of Eq. (35) and an analysis on the derivative of Eq. (35) with respect to δ are discussed in Appendix D.

C. Benchmarking with noninteracting atoms

To provide a meaningful point of comparison for the metrological performance of our setup, we analyze a reference scenario consisting of two identical emitters, each coupled to an independent waveguide. In this configuration, the emitters do not interact and, consequently, their spatial separation does not influence the system dynamics. Hence, if the emitter is prepared in the $|e,g\rangle$ state (as we have assumed in our prior analysis), we can only ascertain the center wavelength of the excited atom. Thus, we seek to sense the center frequency of either atom, $\{\omega_1 = \omega_0 + \frac{\Delta\omega}{2},\ \omega_2 = \omega_0 - \frac{\Delta\omega}{2}\}$, rather than their relative detuning δ. The QFI with respect to ω_m of the joint system, labeled by $H(\omega_m)$, lower bounds the minimum sensitivity of sensing the detuning as $\langle\Delta\delta^2\rangle \geqslant 2/H(\omega_m)$, where the additional factor of 2 arises from the need to perform two separate measurements (one for each atom).

Considering the initial single-excitation state, $|\Psi(t=0)\rangle = \sigma_+^{(m)}|g,g,\{0\}_1,\{0\}_2\rangle$, where $|\{0\}_m\rangle$ represents the waveguide modes coupled to the mth emitter,

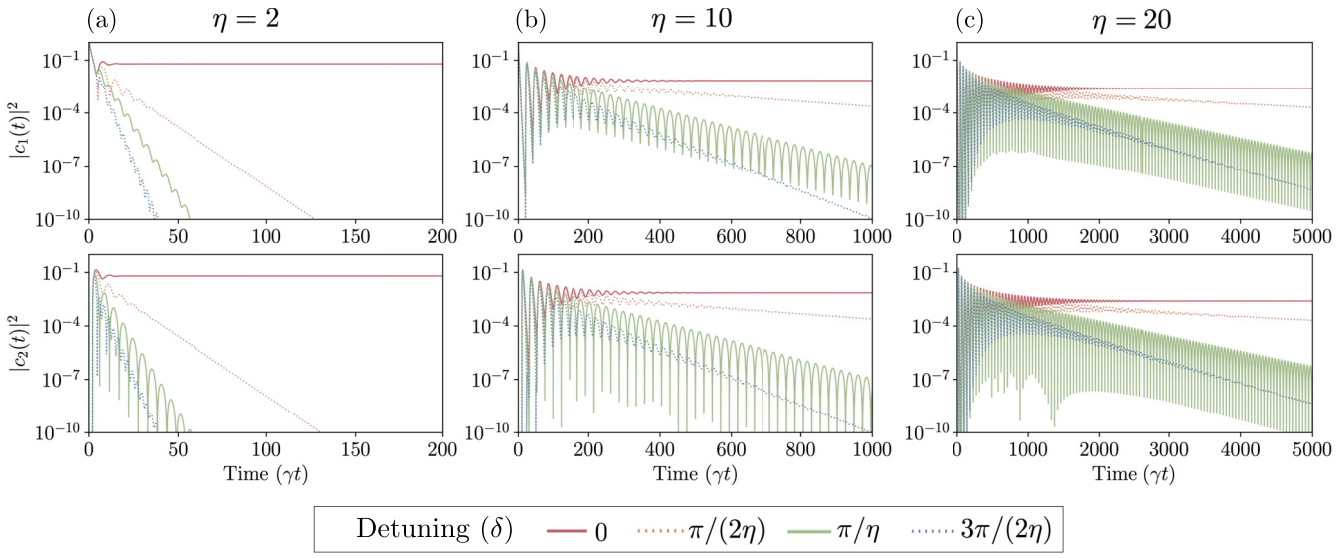


FIG. 6. Emitter dynamics in the presence of detuning for the initial state $|e\rangle_1|g\rangle_2|\{0\}\rangle$ for longer time scales. Emitter excitation probabilities (log-scaled) for emitters 1 and 2 for separation $\eta =$ (a) 2, (b) 10, and (c) 20.

Wigner-Weisskopf theory gives us the joint state

$$|\Psi(t)\rangle = e^{-(\gamma/2+i\omega_m)t}\sigma_+^{(m)}|g,g\rangle \otimes |\{0\}_1,\{0\}_2\rangle + |g,g\rangle \otimes \int_0^t \mathrm{d}\tau\, \xi(\tau)[a_m^\dagger(\tau) + b_m^\dagger(\tau)]\,|\{0\}_1,\{0\}_2\rangle, \tag{37}$$

where $a_m^\dagger(\tau)$, $b_m^\dagger(\tau)$ are creation operations corresponding to left- and right-going temporal modes for the waveguide coupled to emitter m. The photon temporal wave packet is given by $\xi(\tau) = \sqrt{\gamma/2}\,\exp(-(\gamma/2 + i\omega_m)\tau)$.

Since we assume perfect coupling to the waveguide modes, we may use the pure state QFI expression in Eq. (29) evaluated with respect to ω_m (details in Appendix E), which yields

$$H(\omega_m;t) = \frac{4}{\gamma^2}[1 - (e^{-\gamma t} + 2\gamma t)e^{-\gamma t}]. \tag{38}$$

In the limit $t \to \infty$, the QFI becomes $\lim_{t\to\infty} H(\omega_m) = 4/\gamma^2$, which is a constant $H(\tilde{\omega}_m) = 4$, when expressed in the normalized frequency units $\tilde{\omega}_m = \omega_m/\gamma$. The QFI of measuring the center frequency only depends on γ, and is independent of ω_m, and consequently independent of $\Delta\omega$. Thus, the optimal sensitivity for measuring the atomic detuning as obtained from the state of waveguide-coupled emitters surpasses that of independent noninteracting emitters.

VI. CONCLUSIONS AND OUTLOOK

We demonstrate that non-Markovian delay in waveguide QED can be a resource for distributed quantum sensing by investigating a minimal setup of two waveguide-coupled atoms interacting with an external field. The external field introduces a detuning ($\Delta\omega$) between the two emitters, which we aim to sense. We show that the collective non-Markovian and multimode dynamics of the emitters in the presence of detuning exhibits detuning-dependent revivals and suppression of excitations (Fig. 6). The concomitant spectrum of the field radiated by the emitters can be understood in terms of the effective "cavity" formed by the two emitters: When the effective resonances of such a cavity aligns with the emitter resonances, there is an enhanced emission of the radiated field and buildup of the field in the region between the emitters for specific values of the emitter separations ($\eta = \gamma d/v$) and their relative detunings ($\delta = \Delta\omega/\gamma$), given by $\eta\delta \approx (n + \frac{1}{2})\pi$ for $\delta \gtrsim 1$, and $\eta\delta \approx n\pi$ for $\delta \ll 1$ [Fig. 3, and Eqs. (25) and (26)].

Our central result shows that the QFI for estimating the detuning parameter δ, which encodes the field gradient, is enhanced in the presence of non-Markovian delay [Fig. 4(a)]. Such an enhancement is linked to formation of atom-photon quasibound states: Intuitively, the longer the photons spend in "cavity" formed by the atoms and "interrogate" the detuned emitters, the more information can be gained about the detuning parameter. We characterize such atom-photon quasibound states by the rate $\Gamma(t)$ at which the excitation in the emitters + field in the cavity region decays. We identify the minimas in Γ as corresponding to formation of qBIC. The specific parameter values for which we observe peaks in the QFI align with the formation of quasibound states (Figs. 4 and 5): $\eta\delta = (n + \frac{1}{2})\pi$ for $\delta \gtrsim 1$, and $\eta\delta = n\pi$ for $\delta \ll 1$ ($n \in \mathbb{Z}^+$). Further, the formation of qBICs can be understood as arising from an alignment of the atomic resonances with the resonances of the cavity formed by the atoms. Thus, the optimal sensing conditions correspond to delay and detuning parameter values that (1) support formation of quasibound states that facilitate a longer interrogation time, and (2) for long delays, which bring in multiple modes of the environment to probe the collective dynamics of the emitters. Finally, we show that the QFI for estimating the relative atomic detuning as obtained from the non-Markovian collective dynamics of waveguide-coupled emitters exceeds that of two independent emitters by several orders of magnitude.

The optimal (QFI-achieving) measurement will comprise a joint measurement of the waveguide modes and the atomic states. In general, joint projective measurements of the total system (emitters + waveguide modes) can be achieved as

follows: First, a single-excitation-exchange interaction between the emitters and an auxiliary waveguide mode to transduce the state of the emitters; followed by a general multimode unitary interaction and a single-photon measurement. The information about the relative detuning of the atoms is encoded in the collective dynamics of the emitters and, subsequently, in the excitations of the waveguide modes. Given the exponential decay in emitter populations with time, a majority of the detuning information will be encoded in the waveguide modes; as such, we expect the emitter-field transduction to be negligible. The cavitylike resonance features (Fig. 3) indicate that the optimal unitary gate will likely entail temporospectral processing of the waveguide excitation. Remarkably, recent works have shown that in the collective superradiant burst from an atomic ensemble, the temporal mode that carries optimal information, in fact, has a vanishing number of photons [43]. We leave the derivation and constructive formulation of such an optimal measurement for future work.

Given the remarkable experimental progress over recent years, such long-distance waveguide QED regimes can be accessed across various platforms ranging from neutral atoms coupled to optical nanofibers [54–56], circuit QED and giant atoms [57–63], quantum dots coupled to nanophotonic waveguides [64,65], waveguide lattices [66,67], to matter waves in optical lattices [68,69]. Notably, Ref. [69] demonstrated that for ultracold atoms in a vertical one-dimensional optical lattice, emulating waveguide-coupled quantum emitters and photons, the propagation phase of the matter waves emulating photons depends on the gravity gradients. It would be pertinent to explore the role of non-Markovian collective dynamics exhibited in such a system as a resource for sensing gravitational field gradients.

The present framework can be generalized in various ways to further enhance the sensing capabilities of such waveguide QED systems. For example, extending the analysis to multiemitter systems that act as additional probes [12,17,30,70–73]; dispersion engineering to create photonic environments that enable robust quasibound states [74]; and driven emitters that allow for continuous probing of the system [21,72,75]. The present assumptions that the field environment has a flat-spectral density and linear dispersion can be justified for specific platforms, e.g., atoms coupled to an optical nanofiber [76] and superconducting qubits coupled via appropriately engineered Josephson junction arrays [21]. However, generalizing the field spectral density to include nonlinear dispersion and structured reservoirs would open additional mechanisms to realize long-lived atom-photon bound states that can be metrologically advantageous [77]. Indeed, such engineerable dispersion has been realized in experiments with matter waves in optical lattices emulating waveguide QED [69]. Overall, our results establish non-Markovian time-delayed feedback and multimode reservoirs as a resource for distributed quantum sensing, opening new avenues in quantum metrology with waveguide-coupled quantum emitters.

ACKNOWLEDGMENTS

We acknowledge helpful discussions with H. Alaeian, G. Angelatos, A. Clerk, C. N. Gagatsos, D. Schneble, P. Solano, R. Trivedi, and H. E. Türeci. P.D. acknowledges support from Engineering Research Center for Quantum Networks (CQN), awarded by the NSF and DoE under Cooperative Agreement No. 1941583. K.S. acknowledges support from the National Science Foundation under Grant No. PHY-2418249, the Air Force Office of Scientific Research under Award No. FA9550-25-1-0333, the John Templeton Foundation under Award No. 63626, and the U.S. Department of Energy, Office of Science under Grant No. DESC0026059. This work was supported by Grant No. NSF PHY-2309135 to the Kavli Institute for Theoretical Physics (KITP).

This document does not contain technology or technical data controlled under either the U.S. International Traffic in Arms Regulations or the U.S. Export Administration Regulations.

DATA AVAILABILITY

There are no publicly available research data or software supporting this manuscript. Requests for further information or data should be sent to the authors.

APPENDIX A: NON-MARKOVIAN DYNAMICS OF WAVEGUIDE-COUPLED DETUNED EMITTERS

Given the total Hamiltonian [Eqs. (1)–(3)], we derive the following coupled equations of motion for the atomic and field excitation amplitudes defined in Eq. (4):

$$\dot{c}_R(\omega,t) = -i[c_1(t)g^*(\omega)e^{-i\omega x_1/v}e^{i(\omega-\omega_1)t} + c_2(t)g^*(\omega)e^{-i\omega x_2/v}e^{i(\omega-\omega_2)t}], \tag{A1a}$$

$$\dot{c}_L(\omega,t) = -i[c_1(t)g^*(\omega)e^{i\omega x_1/v}e^{i(\omega-\omega_1)t} + c_2(t)g^*(\omega)e^{i\omega x_2/v}e^{i(\omega-\omega_2)t}], \tag{A1b}$$

$$\dot{c}_m(t) = -i\int_0^\infty \mathrm{d}\omega\, g(\omega)e^{-i(\omega-\omega_m)t}[c_R(\omega,t)e^{i\omega x_m/v} + c_L(\omega,t)e^{-i\omega x_m/v}], \quad m=\{1,2\}. \tag{A1c}$$

Integrating Eqs. (A1a) and (A1b) yields

$$c_R(\omega,t) = -ig^*(\omega)\int_0^t \mathrm{d}\tau[c_1(\tau)e^{-i\omega x_1/v}e^{i(\omega-\omega_1)\tau} + c_2(\tau)e^{-i\omega x_2/v}e^{i(\omega-\omega_2)\tau}], \tag{A2}$$

$$c_L(\omega,t) = -ig^*(\omega)\int_0^t \mathrm{d}\tau[c_1(\tau)e^{i\omega x_1/v}e^{i(\omega-\omega_1)\tau} + c_2(\tau)e^{i\omega x_2/v}e^{i(\omega-\omega_2)\tau}]. \tag{A3}$$

Substituting the above into the emitters' equation of motion [Eq. (A1c)] gives the coupled dynamical equations for the two atoms [Eqs. (5) and (6)]. The corresponding Laplace-transformed excitation amplitudes $\mathcal{C}_{1,2}(s)$ are

$$\gamma\mathcal{C}_1(\tilde{s}) = \frac{c_1(0)(\tilde{s}-i\delta+1/2) - c_2(0)e^{i\phi_1}e^{-\eta\tilde{s}}/2}{(\tilde{s}+1/2)(\tilde{s}-i\delta+1/2) - (e^{i\phi_1}e^{-\eta\tilde{s}}/2)^2}, \tag{A4a}$$

$$\gamma\mathcal{C}_2(\tilde{s}) = \frac{c_2(0)(\tilde{s}+i\delta+1/2) - c_1(0)e^{i\phi_2}e^{-\eta\tilde{s}}/2}{(\tilde{s}+1/2)(\tilde{s}+i\delta+1/2) - (e^{i\phi_2}e^{-\eta\tilde{s}}/2)^2}, \tag{A4b}$$

which yield Eqs. (7) and (8) for the given initial conditions ($c_1(0)=1$, $c_2(0)=0$). We now detail the solutions to the coupled atomic dynamics, as obtained from taking the inverse Laplace transform of the above Laplace coefficients using two approaches.

1. Atomic dynamics: Series solution

We solve the coupled dynamics of the atoms by expanding the denominators in the Laplace coefficients in terms of a series, which physically corresponds to an expansion in terms of the number of photon wave packet oscillations. We rewrite the Laplace coefficient $\mathcal{C}_2(s)$ in Eq. (A4b) as

$$\gamma\mathcal{C}_2(s) = \frac{-\beta e^{i\phi_2}e^{-\eta\tilde{s}}/2}{(\tilde{s}+1/2)(\tilde{s}+i\delta+1/2)}\left[1 - \frac{\beta^2(e^{i\phi_2}e^{-\eta\tilde{s}}/2)^2}{(\tilde{s}+1/2)(\tilde{s}+i\delta+1/2)}\right]^{-1} \tag{A5}$$

$$= -\sum_{n=0}^{\infty}\frac{\beta^{2n+1}e^{i(2n+1)\phi_2}}{2^{2n+1}}\frac{e^{-(2n+1)\eta\tilde{s}}}{(\tilde{s}+1/2)^{n+1}(\tilde{s}+i\delta+1/2)^{n+1}}. \tag{A6}$$

To invert the above Laplace coefficient, we utilize the following Laplace transform relations [78]:

$$e^{-sa}F(s) \xrightarrow{\mathcal{L}^{-1}} f(t-a)\Theta(t-a), \tag{A7a}$$

$$\frac{\Gamma(n)}{(s+a)^n(s+b)^n} \xrightarrow{\mathcal{L}^{-1}} \sqrt{\pi}\left(\frac{t}{a-b}\right)^{n-1/2}e^{-(a+b)t/2}I_{n-1/2}\left(\frac{a-b}{2}t\right), \quad (n>0), \tag{A7b}$$

where I_n is the modified Bessel function of the first kind and $\Gamma(n)=(n-1)!$ is the Gamma function. Using these relations in Eq. (A6) yields the time dynamics of atom 2, which is given by

$$c_2(t) = -\sqrt{\pi}e^{-i\delta\gamma t/2}\sum_{n=0}^{\infty}\frac{\beta^{2n+1}e^{i(2n+1)(\phi_1+\phi_2)/2}}{2^{2n+1}n!}e^{-(\gamma t-(2n+1)\eta)/2}\Theta[\gamma t-(2n+1)\eta]$$
$$\times\left(\frac{\gamma t-(2n+1)\eta}{i\delta}\right)^{n+1/2}I_{n+1/2}\left(\frac{i\delta(\gamma t-(2n+1)\eta)}{2}\right). \tag{A8}$$

This yields Eq. (11) with the coefficient $\Xi_n^{(2)}(t)$:

$$\Xi_n^{(2)}(t) \equiv -\frac{\sqrt{\pi}}{2^{2n+1}n!}\left(\frac{\gamma t-(2n+1)\eta}{i\delta}\right)^{n+1/2}I_{n+1/2}\left(\frac{i\delta(\gamma t-(2n+1)\eta)}{2}\right). \tag{A9}$$

We now use Eq. (6) to determine the excitation amplitude for the first atom, $c_1(t)$, in terms of $c_2(t)$. For $t<d/v$, we get $c_1(t)=c_1(0)e^{-\gamma t/2}$, i.e., atomic decay due to spontaneous emission. For $t>d/v$, we have instead

$$c_1(t) = -\frac{1}{\beta}e^{-i\phi_1}e^{i\delta(\gamma t+\eta)}c_2(\gamma t+\eta) - \frac{2}{\gamma\beta}e^{-i\phi_1}e^{i\delta(\gamma t+\eta)}\dot{c}_2(\gamma t+\eta). \tag{A10}$$

We use the recursive definition of the derivative of modified Bessel functions from Ref. [79] to simplify the derivative $\dot{c}_2(t+d/v)$:

$$2\frac{\mathrm{d}}{\mathrm{d}z}I_n(z) = I_{n+1}(z) + I_{n-1}(z). \tag{A11}$$

We thus obtain the expression for $c_1(t)$:

$$c_1(t) = e^{-\gamma t/2} + \sqrt{\pi}e^{i\delta\gamma t/2}\sum_{n=1}^{\infty}\frac{\beta^{2n}e^{in(\phi_1+\phi_2)}}{2^{2n+1}n!}\Theta(\gamma t-2n\eta)e^{-(\gamma t-2n\eta)/2}\left(\frac{\gamma t-2n\eta}{i\delta}\right)^{n-1/2}\left[\left\{\frac{2n+1}{i\delta}-(\gamma t-2n\eta)\right\}\right.$$
$$\left.\times I_{n+1/2}\left(\frac{i\delta(\gamma t-2n\eta)}{2}\right) + \left(\frac{\gamma t-2n\eta}{2}\right)\left\{I_{n+3/2}\left(\frac{i\delta(\gamma t-2n\eta)}{2}\right) + I_{n-1/2}\left(\frac{i\delta(\gamma t-2n\eta)}{2}\right)\right\}\right]. \tag{A12}$$

This results in Eq. (10) with the coefficient $\Xi_n^{(1)}(t)$ defined as

$$\Xi_n^{(1)}(t) \equiv \frac{\sqrt{\pi}}{2^{2n+1}n!}\Bigg[\left(\frac{2n+1}{i\delta}\right)\left(\frac{\gamma t-2n\eta}{i\delta}\right)^{n-1/2} I_{n+1/2}\left(\frac{i\delta(\gamma t-2n\eta)}{2}\right) - i\delta\left(\frac{\gamma t-2n\eta}{i\delta}\right)^{n+1/2} I_{n+1/2}\left(\frac{i\delta(\gamma t-2n\eta)}{2}\right)$$
$$+\frac{i\delta}{2}\left(\frac{\gamma t-2n\eta}{i\delta}\right)^{n+1/2}\left\{I_{n+3/2}\left(\frac{i\delta(\gamma t-2n\eta)}{2}\right)+I_{n-1/2}\left(\frac{i\delta(\gamma t-2n\eta)}{2}\right)\right\}\Bigg]. \tag{A13}$$

2. Atomic dynamics: Multiexponential decay

As an alternate approach for solving the atomic dynamics, one can invert Eqs. (A4a) and (A4b) using Cauchy's residue theorem. In order to apply Cauchy's residue theorem, we need to numerically evaluate the poles of Eqs. (A4a) and (A4b), i.e., determine the roots of the denominators,

$$f_1(\tilde{s};\delta) = (\tilde{s}+1/2)(\tilde{s}-i\delta+1/2) - \beta^2(e^{i\phi_1}e^{-\eta\tilde{s}}/2)^2, \tag{A14a}$$

$$f_2(\tilde{s};\delta) = (\tilde{s}+1/2)(\tilde{s}+i\delta+1/2) - \beta^2(e^{i\phi_2}e^{-\eta\tilde{s}}/2)^2. \tag{A14b}$$

We note that for $\delta = 0$, $f_m(\tilde{s};\delta) = 0$ resemble the transcendental equation $we^w = z$. Hence, the solutions to $f_m(\tilde{s};0) = 0$ are given by the Lambert W function solutions,

$$\tilde{s}_{\pm,k}^{(m)} = \frac{1}{\eta}W_k\left(\pm\frac{\eta\beta}{2}\exp(i\phi_j+\eta/2)\right) - \frac{1}{2} \equiv \tilde{s}_{\sigma,k}^{(m)}, \tag{A15}$$

where the superscript $m = 1, 2$ is the atomic index, while the subscripts $\sigma \in \{+,-\}$ and $k \in \mathbb{Z}$ denote the branch of the Lambert W solution. For the sake of brevity, we adopt a joint subscript notation $\boldsymbol{j} \equiv (\sigma, j)$, where $\sigma \in \{+,-\}$ and $j \in \mathbb{Z}$ for the residues and poles in the rest of the Appendixes as well as the main text.

However, for $\delta \neq 0$, the equations no longer have the standard transcendental form. The general solutions are expected to be perturbations (proportional to δ) of $\tilde{s}_{\boldsymbol{k}}^{(m)}$.

Given a solution $\tilde{s}_{\boldsymbol{k}}^{(m)} = \tilde{s}_0$ for the equation $f_m(\tilde{s};0) = 0$, let us assume that the roots of $f_m(\tilde{s};\delta)$ are of the form $\tilde{s}_0+\alpha$, where $\alpha \in \mathbb{C}$ is δ and pole index k dependent, with no analytic closed form. We use the properties for Lambert W functions to derive the equivalent transcendental equation (for $\beta = 1$)

$$\begin{aligned} f_m(\tilde{s}_0+\alpha;\delta) = 0 &\Rightarrow (\tilde{s}_0+\alpha+1/2)(\tilde{s}_0+\alpha\pm i\delta+1/2) - (e^{i\phi_j}e^{-\eta(\tilde{s}_0+\alpha)}/2)^2 = 0 \\ &\Rightarrow \alpha^2 + 2\alpha(\tilde{s}_0+1/2) + (1-e^{-2\eta\alpha})(\tilde{s}_0+1/2)^2 \pm i\delta(\tilde{s}_0+\alpha+1/2) = 0, \end{aligned} \tag{A16}$$

where we use the relation $[\exp(i\phi_j-\eta\tilde{s}_0)/2]^2 = (\tilde{s}_0+1/2)^2$ to replace the exponential with a polynomial term. This is a reframed transcendental equation in terms of the shift variable α.

The corresponding residues $R_{\sigma,j}^{(m)}$ for the jth pole associated with the inverse Laplace transform of $\mathcal{C}^{(m)}$ is

$$R_{\sigma,j}^{(m)} = \frac{c_m(0)\left(\tilde{s}_{\sigma,j}^{(m)}+(-1)^m i\delta+1/2\right) - c_{m'}(0)e^{i\phi_m}e^{-\eta\tilde{s}_{\sigma,j}^{(m)}}/2}{1+2\tilde{s}_{\sigma,j}^{(m)}+(-1)^m i\delta+\eta\left(e^{2i\phi_n-2\eta\tilde{s}_{\sigma,j}^{(m)}}/2\right)}. \tag{A17}$$

For the numerical evaluation of the poles, we solve Eq. (A16) to determine the δ-dependent shifts to the Lambert-W-based solutions. This technique is numerically more stable since $|\alpha|$ is typically a small number, where we find $|\alpha/(\tilde{s}_0+1/2)| \sim \mathcal{O}(1)$. The scaling of α can be determined by evaluating roots of the approximate polynomial equation for Eq. (A16), obtained by a Taylor expansion of the $e^{-\eta\alpha}$ term. Additionally, since we evaluate the shift for every branch of the Lambert W function, we avoid inadvertently skipping poles that contribute to the overall system evolution. We use Muller's root-finding algorithm for our numerics. For all the numerical evaluations in this article, we use relative error tolerance $\epsilon \leqslant 10^{-7}$, maximum iteration count $N = 10^4$, and choose initial shifts $x_{\{0,1,2\}} = \{-0.05, -0.01, -0.01i\} \times \delta/\eta$ to obtain stable numerical solutions.

APPENDIX B: ATOMIC FREQUENCY RESPONSE AND SPECTRUM OF THE EMITTED FIELD

The frequency response functions for each atom are defined as the Fourier transform of the atomic amplitudes $F_m(\tilde{\omega}) \equiv \int \mathrm{d}t\, c_m(t)e^{i(\tilde{\omega}-\tilde{\omega}_m)\gamma t}$. These can be related to the Laplace coefficients in Eqs. (7) and (8) as follows:

$$\gamma F_1(\tilde{\omega}) = \gamma\mathcal{C}_1(-i(\tilde{\omega}-\tilde{\omega}_1)) = \frac{c_1(0)(-i(\tilde{\omega}-\tilde{\omega}_1)-i\delta+1/2) - c_2(0)e^{i\phi_1}e^{i\eta(\tilde{\omega}-\tilde{\omega}_1)}/2}{(-i(\tilde{\omega}-\tilde{\omega}_1)+1/2)(-i(\tilde{\omega}-\tilde{\omega}_1)-i\delta+1/2) - (e^{i\phi_1}e^{i\eta(\tilde{\omega}-\tilde{\omega}_1)}/2)^2}, \tag{B1}$$

$$\gamma F_2(\tilde{\omega}) = \gamma\mathcal{C}_2(-i(\tilde{\omega}-\omega_2)) = \frac{c_2(0)(-i(\tilde{\omega}-\omega_2)+i\delta+1/2) - c_1(0)e^{i\phi_2}e^{i\eta(\tilde{\omega}-\omega_2)}/2}{(-i(\tilde{\omega}-\omega_2)+1/2)(-i(\tilde{\omega}-\omega_2)+i\delta+1/2) - (e^{i\phi_2}e^{i\eta(\tilde{\omega}-\omega_2)}/2)^2}. \tag{B2}$$

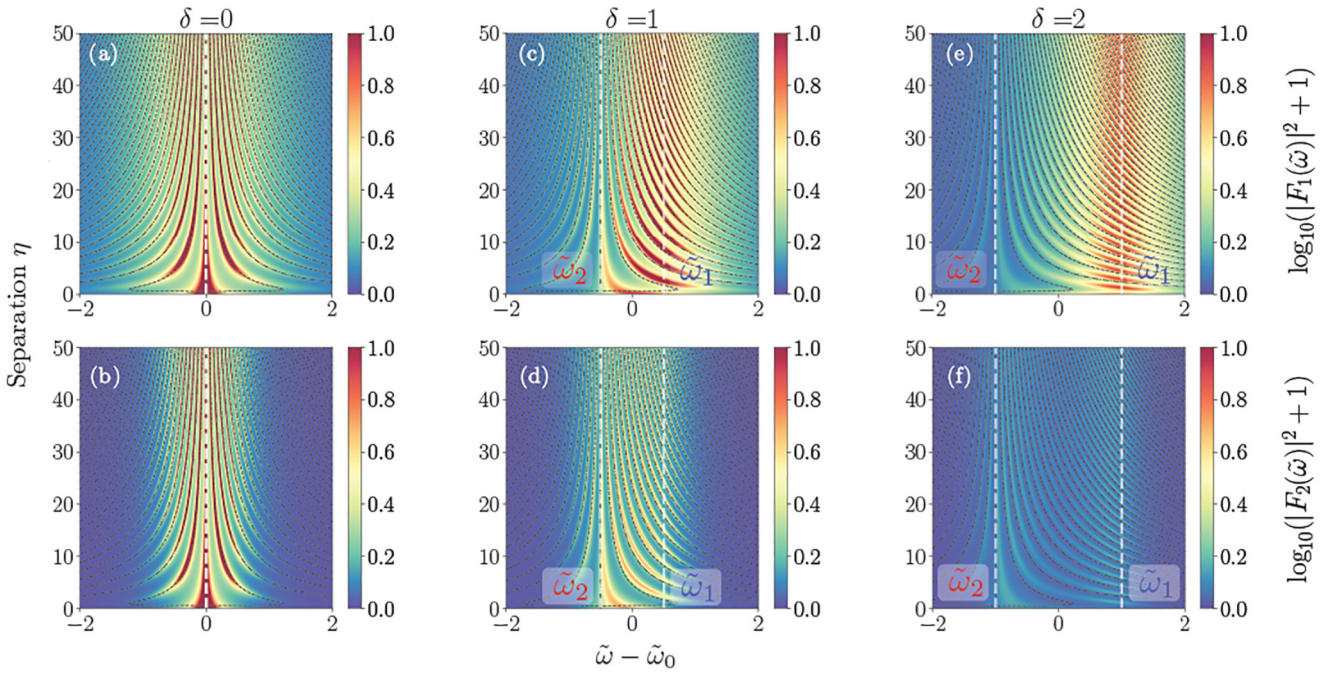


FIG. 7. Atomic spectral response functions $F_{1,2}(\tilde{\omega})$ as a function of frequency $\tilde{\omega}-\tilde{\omega}_0$ and interatomic separation η for different values of detunings δ: $\delta=0$ for panels (a) and (b); $\delta=1$ for panels (c) and (d); and $\delta=2$ for panels (e) and (f). The first row [panels (a), (c), and (e)] shows the response functions for atom 1 $[F_1(\tilde{\omega})]$, while the second row shows the response functions for atom 2 $[F_2(\tilde{\omega})]$. The vertical white dashed lines indicate the frequencies of the two emitters. The black dash-dotted and dashed curves in Fig. 7 correspond to the frequencies $\tilde{\omega}^+_{n\delta}-\tilde{\omega}_0$ and $\tilde{\omega}^-_{n\delta}-\tilde{\omega}_0$, given by Eq. (24), respectively. Note that we have restricted the range of z axis to keep consistent colorbar values for all plots for qualitative illustration. The z ranges for the plots go above and below the set limits.

For the given initial state $(c_1(0)=1,\ c_2(0)=0)$, the above expressions simplify to Eqs. (18) and (19). Substituting $\bar{\omega}\equiv\tilde{\omega}-\tilde{\omega}_0$, we get

$$\gamma F_1(\bar{\omega})=\frac{-i(\bar{\omega}+\delta/2)+1/2}{D(\bar{\omega})}, \tag{B3}$$

$$\gamma F_2(\bar{\omega})=-\frac{e^{i\eta\bar{\omega}}e^{i\eta\delta/2}/2}{D(\bar{\omega})}, \tag{B4}$$

where the denominator $D(\bar{\omega})$ is given by

$$D(\bar{\omega})=\left[-i\bar{\omega}+\frac{1}{2}\right]^2+\frac{\delta^2}{4}-\frac{e^{2i\eta\bar{\omega}}e^{i\eta\delta}}{4}. \tag{B5}$$

Figure 7 shows the atomic response functions for different detuning values. We note that the frequency response of emitter 1 $[F_1(\tilde{\omega})]$ is peaked at its resonance $\tilde{\omega}_1$, while that for emitter 2 $[F_2(\tilde{\omega})]$ exhibits peaks at both $\tilde{\omega}_1$ and $\tilde{\omega}_2$.

1. Field spectrum

The emitted field spectrum $G(\tilde{\omega})$, in the steady state, is given by

$$\begin{aligned}G(\tilde{\omega})&\equiv|c_R(\tilde{\omega},\infty)|^2+|c_L(\tilde{\omega},\infty)|^2\\&=\frac{\gamma}{\pi}(|F_1(\tilde{\omega})|^2+|F_2(\tilde{\omega})|^2\\&\quad+2\cos(\tilde{\omega}\eta)\mathrm{Re}[F_1^*(\tilde{\omega})F_2(\tilde{\omega})]).\end{aligned} \tag{B6}$$

Shifting the frequency axis to be centered at $\tilde{\omega}_0$, the explicit expression for the spectrum becomes

$$\begin{aligned}G(\bar{\omega})=\frac{\gamma}{\pi}[&|F_1(\bar{\omega})|^2+|F_2(\bar{\omega})|^2+2\cos((\bar{\omega}+\tilde{\omega}_0)\eta)\\&\times\mathrm{Re}[F_1^*(\bar{\omega})F_2(\bar{\omega})]].\end{aligned} \tag{B7}$$

Using the condition

$$\tilde{\omega}_0\eta=\tilde{\omega}_2\eta+\frac{\delta\eta}{2}=\phi_2+\frac{\delta\eta}{2}=2p\pi+\frac{\delta\eta}{2}, \tag{B8}$$

assuming the propagation phase $\phi_2=2p\pi$ [Eq. (14)], we get

$$\begin{aligned}G(\bar{\omega})=\frac{\gamma}{\pi}\Bigg[&|F_1(\bar{\omega})|^2+|F_2(\bar{\omega})|^2\\&+2\cos\left(\bar{\omega}\eta+\frac{\delta\eta}{2}\right)\mathrm{Re}[F_1^*(\bar{\omega})F_2(\bar{\omega})]\Bigg].\end{aligned} \tag{B9}$$

2. Spectrum peaks in presence of detuning

Equating the approximate peaks of the spectrum obtained via Eq. (24) to the resonance frequency of emitter 1, we get the following transcendental relation between the detuning δ and the atomic separation η_n:

$$\tilde{\omega}^{\pm}_{n\delta}=\tilde{\omega}_1 \tag{B10}$$

$$\Rightarrow\tilde{\omega}_0-\frac{\delta}{2}+\frac{1}{\eta_n}\mathrm{Im}\left[W_n\left(\pm\frac{\eta_n}{2}e^{\eta_n/2}\right)\right]=\tilde{\omega}_0+\frac{\delta}{2} \tag{B11}$$

$$\Rightarrow\mathrm{Im}\left[W_n\left(\pm\frac{\eta_n}{2}e^{\eta_n/2}\right)\right]=\delta\eta_n. \tag{B12}$$

In order to simplify the left-hand side of the above relation, let us define

$$z_n^{\pm} \equiv \pm\frac{\eta_n}{2}e^{\eta_n/2}. \tag{B13}$$

For large atomic separations ($\eta_n \gtrsim 1$), $|z_n^{\pm}|$ is also large such that the Lambert W function admits the asymptotic expansion [80]:

$$W_n(z_n^{\pm}) \approx \ln(z_n^{\pm}) + 2in\pi - \ln[\ln(z_n^{\pm}) + 2in\pi]. \tag{B14}$$

The imaginary part of the above simplifies to

$$\mathrm{Im}[W_n(z_n^{+})] \approx \mathrm{Im}\left[\frac{\eta_n}{2} + \ln\left(\frac{\eta_n}{2}\right) + 2in\pi - \ln\left[\frac{\eta_n}{2} + \ln\left(\frac{\eta_n}{2}\right) + 2in\pi\right]\right] \tag{B15}$$

$$\Rightarrow \mathrm{Im}[W_n(z_n^{+})] \approx 2n\pi - \tan^{-1}\left(\frac{2n\pi}{\eta_n/2 + \ln(\eta_n/2)}\right), \tag{B16}$$

where we have used the simplification $\mathrm{Im}[\ln(x+iy)] = \mathrm{Im}[\ln(\sqrt{x^2+y^2}e^{i\tan^{-1}(y/x)})] = \tan^{-1}(y/x)$ in the second step.

Similarly for $\mathrm{Im}[W_n(z_-)]$, we have

$$\mathrm{Im}[W_n(z_n^{-})] \approx \mathrm{Im}\left[\frac{\eta_n}{2} + \ln\left(\frac{\eta_n}{2}\right) + i(2n+1)\pi - \ln\left[\frac{\eta_n}{2} + \ln\left(\frac{\eta_n}{2}\right) + i(2n+1)\pi\right]\right] \tag{B17}$$

$$\Rightarrow \mathrm{Im}[W_n(z_n^{-})] \approx (2n+1)\pi - \tan^{-1}\left(\frac{(2n+1)\pi}{\eta_n/2 + \ln(\eta_n/2)}\right). \tag{B18}$$

To further simplify the above expressions, we consider two parameter regimes:

(1) Large detunings, $\delta > 1$: For $\delta > 1$, such that emitter detunings are larger than their respective linewidths, a large number (n) of branches of the Lambert W function $W_n(z_n^{\pm})$ are required to describe the spectrum of the field close to the emitter resonances. This can be seen qualitatively from Fig. 3. Thus, for $\delta \gtrsim 1$, the heuristic relation $\delta\eta_n \sim n\pi$ implies that $n\pi \gtrsim \eta_n$. In this regime, $\tan^{-1}(\frac{2n\pi}{\eta_n/2+\ln(\eta_n/2)}) \approx \pi/2$, such that Eqs. (B16) and (B18) simplify to

$$\mathrm{Im}[W_n(z_n^{+})] \approx \left(2n - \tfrac{1}{2}\right)\pi \Rightarrow \delta\eta_n \approx \left(2n - \tfrac{1}{2}\right)\pi, \tag{B19}$$

$$\mathrm{Im}[W_n(z_n^{-})] \approx \left(2n + \tfrac{1}{2}\right)\pi \Rightarrow \delta\eta_n \approx \left(2n + \tfrac{1}{2}\right)\pi, \tag{B20}$$

where we have used Eq. (B12). Combining the above two conditions, we get Eq. (25).

(2) Small detunings, $\delta \ll 1$: For small emitter detunings, the corresponding values of n for the Lambert W function branches needed to describe the spectrum of the field near emitter resonances are small. Thus, for $\delta \ll 1$, the heuristic relation $\delta\eta_n \sim n\pi$ implies that $n\pi \ll \eta_n$. In this regime, $\tan^{-1}(\frac{2n\pi}{\eta_n/2+\ln(\eta_n/2)}) \approx 0$, such that Eqs. (B16) and (B18) yield

$$\mathrm{Im}[W_n(z_n^{+})] \approx 2n\pi \Rightarrow \delta\eta_n \approx 2n\pi, \tag{B21}$$

$$\mathrm{Im}[W_n(z_n^{-})] \approx (2n+1)\pi \Rightarrow \delta\eta_n \approx (2n+1)\pi. \tag{B22}$$

The above equations combined give us the condition

$$\eta_n\delta \approx n\pi, \tag{B23}$$

yielding Eq. (26).

For both cases, the difference between adjacent peaks of the spectrum is [from Eqs. (24), (B19)–(B22)]

$$|\tilde{\omega}_{n\delta}^{+} - \tilde{\omega}_{n\delta}^{-}| = \frac{1}{\eta}\left|\mathrm{Im}\left[W_n\left(\frac{\eta_n}{2}e^{\eta_n/2}\right) - W_n\left(-\frac{\eta_n}{2}e^{\eta_n/2}\right)\right]\right| \approx \frac{\pi}{\eta}. \tag{B24}$$

This yields Eq. (27).

APPENDIX C: QUANTUM FISHER INFORMATION EVALUATION

We know that for a single parameter family of states ρ_θ, the QFI can be directly calculated using the symmetric logarithmic derivative (SLD) L_θ by the relation

$$H(\theta) = \mathrm{Tr}\left[\rho_\theta L_\theta^2\right]. \tag{C1}$$

The SLD is implicitly defined by $\partial\rho_\theta/\partial\theta = (\rho_\theta L_\theta + L_\theta\rho_\theta)/2$. For pure states, i.e., states whose density matrix obeys $\rho_\theta^2 = \rho_\theta$ [51], we note that

$$\frac{\partial\rho_\theta}{\partial\theta} = \frac{\partial\rho_\theta^2}{\partial\theta} = \rho_\theta\frac{\partial\rho_\theta}{\partial\theta} + \frac{\partial\rho_\theta}{\partial\theta}\rho_\theta. \tag{C2}$$

Thus, in this case $2\partial\rho_\theta/\partial\theta$ is the same as L_θ. The quantum Fisher information is then

$$H(\theta) = \mathrm{Tr}\left[\rho_\theta L_\theta^2\right] = 4\mathrm{Tr}\rho_\theta\left(\frac{\partial\rho_\theta}{\partial\theta}\right)^2 \tag{C3}$$

$$= 4[\mathrm{Re}\langle\partial_\theta\psi_\theta \mid \partial_\theta\psi_\theta\rangle + \langle\psi_\theta \mid \partial_\theta\psi_\theta\rangle^2]. \tag{C4}$$

For the present article, we seek to evaluate $H(\delta)$ to obtain bounds for sensing the atomic detuning. We define $\tilde{\omega}_1 = \tilde{\omega}_0 + \delta/2$ and $\tilde{\omega}_2 = \tilde{\omega}_0 - \delta/2$. Thus, for $|\partial_\delta\Psi(t)\rangle$, we have

$$\frac{\partial|\Psi_{\delta,\eta}(\tilde{t})\rangle}{\partial\delta} = \sum_{m=1,2}\partial_\delta c_m(\tilde{t})\hat{\sigma}_+^{(m)}|g,g,\{0\}\rangle + \int_0^\infty \mathrm{d}\tilde{\omega}\,[\partial_\delta c_R(\tilde{\omega},\tilde{t})\hat{a}_R^\dagger(\tilde{\omega}) + \partial_\delta c_L(\tilde{\omega},\tilde{t})b^\dagger(\tilde{\omega})]|g,g,\{0\}\rangle. \tag{C5}$$

We now have to evaluate $\partial_\delta c_1(\tilde{t})$, $\partial_\delta c_2(\tilde{t})$ based on Eq. (A17). We note that based on our numerical evaluation techniques for the poles in Appendix A, the poles $\tilde{s}_{\boldsymbol{k}}^{(m)}$ can be expressed as $\tilde{s}_{\boldsymbol{k}}^{(m)} = \bar{s}_{\boldsymbol{k}}^{(m)} + \alpha_{\boldsymbol{k}}^{(m)}(\delta)$, where $\bar{s}_{\boldsymbol{k}}^{(m)}$ is the $\delta = 0$ solution and $\alpha_{\boldsymbol{k}}^{(1)}(\delta)$ is the δ-dependent perturbation. As a reminder, we use the compact joint index $\boldsymbol{k} = (\sigma, k) \in \{+,-\}\times\mathbb{Z}$, where we truncate $|k| \leqslant 250$ for numerical evaluations.

We may take a partial derivative of the transcendental equation [Eq. (A16)] to get

$$2\alpha_k^{(1)}(\delta)\partial_\delta\big[\alpha_k^{(1)}(\delta)\big] + 2\big[\bar{s}_k^{(1)} + 1/2\big]\partial_\delta\big[\alpha_k^{(1)}(\delta)\big] + 2\eta\beta^2\big(\bar{s}_k^{(1)} + 1/2\big)^2 e^{-2\eta\alpha_k^{(1)}(\delta)}\partial_\delta\big[\alpha_k^{(1)}(\delta)\big] - i\big(\bar{s}_k^{(1)} + \alpha_k^{(1)}(\delta) + 1/2\big) - i\delta\partial_\delta\big[\alpha_k^{(1)}(\delta)\big] = 0. \tag{C6}$$

From which, we obtain

$$\partial_\delta\big[\alpha_k^{(1)}(\delta)\big] = \frac{i\big(\bar{s}_k^{(1)} + \alpha_k^{(1)}(\delta) + 1/2\big)}{2\alpha_k^{(1)}(\delta) + 2\big[\bar{s}_k^{(1)} + 1/2\big] + 2\eta\beta^2\big(\bar{s}_k^{(1)} + 1/2\big)^2 e^{-2\eta\alpha_k^{(1)}(\delta)} - i\delta}. \tag{C7}$$

Similarly,

$$\partial_\delta\big[\alpha_k^{(2)}(\delta)\big] = \frac{-i\big(\bar{s}_k^{(2)} + \alpha_k^{(2)}(\delta) + 1/2\big)}{2\alpha_k^{(2)}(\delta) + 2\big[\bar{s}_k^{(2)} + 1/2\big] + 2\eta\beta^2\big(\bar{s}_k^{(2)} + 1/2\big)^2 e^{-2\eta\alpha_k^{(2)}(\delta)} + i\delta}. \tag{C8}$$

Hence, we may write $\partial_\delta c_1(\tilde{t})$ as

$$\begin{aligned}\partial_\delta c_1(\tilde{t}) &= \sum_k \left[\frac{\mathcal{A}_{1,k} - \mathcal{B}_{1,k}}{\big(1 + 2\tilde{s}_k^{(1)} - i\delta + \beta^2\eta(e^{2i\phi_2 - 2\eta\tilde{s}_k^{(1)}}/2)\big)^2} + R_k^{(1)}\partial_\delta\big[\alpha_k^{(1)}(\delta)\big]\right]\exp\big(\tilde{s}_k^{(1)}t\big)\\ &\equiv \sum_k \mathcal{R}_k^{(1)}\exp\big(\tilde{s}_k^{(1)}t\big),\end{aligned} \tag{C9}$$

where $\mathcal{A}_{1,k}$ and $\mathcal{B}_{1,k}$ are

$$\mathcal{A}_{1,k} = \big[c_1(0)\big(\partial_\delta\big[\alpha_k^{(1)}(\delta)\big] - i\big) - \beta c_2(0)e^{i\phi_1 - \eta\tilde{s}_k^{(1)}}\big(i\eta/2 - \eta\partial_\delta\big[\alpha_k^{(1)}(\delta)\big]\big)/2\big]\big(1 + 2\tilde{s}_k^{(1)} - i\delta + \beta^2\eta(e^{2i\phi_2 - 2\eta\tilde{s}_k^{(1)}}/2)\big), \tag{C10a}$$

$$\mathcal{B}_{1,k} = \big(c_1(0)\big(\tilde{s}_k^{(1)} - i\delta + 1/2\big) - \beta c_2(0)e^{i\phi_1}e^{-\eta\tilde{s}_k^{(1)}}/2\big)\big[2\partial_\delta\big[\alpha_k^{(1)}(\delta)\big] - i + \beta^2\eta(e^{2i\phi_2 - 2\eta\tilde{s}_k^{(1)}}/2)\big(-i\eta - 2\eta\partial_\delta\big[\alpha_k^{(1)}(\delta)\big]\big)\big]. \tag{C10b}$$

Similarly, we have

$$\begin{aligned}\partial_\delta c_2(\tilde{t}) &= \sum_k \left[\frac{\mathcal{A}_{2,k} - \mathcal{B}_{2,k}}{\big(1 + 2\tilde{s}_k^{(2)} + i\delta + \beta^2\eta\big(e^{2i\phi_1 - 2\eta\tilde{s}_k^{(2)}}/2\big)\big)^2} + R_k^{(2)}\partial_\delta\big[\alpha_k^{(2)}(\delta)\big]\right]\exp\big(\tilde{s}_k^{(2)}t\big)\\ &\equiv \sum_k \mathcal{R}_k^{(2)}\exp\big(\tilde{s}_k^{(2)}t\big),\end{aligned} \tag{C11}$$

where $\mathcal{A}_{2,k}$ and $\mathcal{B}_{2,k}$ are

$$\mathcal{A}_{2,k} = \big[c_2(0)\big(\partial_\delta\big[\alpha_k^{(2)}(\delta)\big] + i\big) - \beta c_1(0)e^{i\phi_2 - \eta\tilde{s}_k^{(2)}}\big(-i\eta/2 - \eta\partial_\delta\big[\alpha_k^{(2)}(\delta)\big]\big)/2\big]\big(1 + 2\tilde{s}_k^{(2)} + i\delta + \beta^2\eta\big(e^{2i\phi_1 - 2\eta\tilde{s}_k^{(2)}}/2\big)\big), \tag{C12a}$$

$$\mathcal{B}_{2,k} = \big(c_2(0)\big(\tilde{s}_k^{(2)} + i\delta + 1/2\big) - \beta c_1(0)e^{i\phi_2}e^{-\eta\tilde{s}_k^{(2)}}/2\big)\big[2\partial_\delta\big[\alpha_k^{(2)}(\delta)\big] + i + \beta^2\eta(e^{2i\phi_1 - 2\eta\tilde{s}_k^{(2)}}/2)\big(i\eta - 2\eta\partial_\delta\big[\alpha_k^{(1)}(\delta)\big]\big)\big]. \tag{C12b}$$

The derivatives of the field amplitudes can be calculated from

$$\partial_\delta c_R(\omega,t) = -i\sum_k \int_0^t \mathrm{d}\tau\, g^*(\omega)\left[\left(\mathcal{R}_k^{(1)} - i\frac{\tau}{2}R_k^{(1)}\right)e^{\tilde{s}_k^{(1)}\tau}e^{-i\omega x_1/v}e^{i(\omega-\omega_1)\tau} + \left(\mathcal{R}_k^{(2)} + i\frac{\tau}{2}R_k^{(2)}\right)e^{\tilde{s}_k^{(2)}\tau}e^{-i\omega x_2/v}e^{i(\omega-\omega_2)\tau}\right], \tag{C13a}$$

$$\partial_\delta c_L(\omega,t) = -i\sum_k \int_0^t \mathrm{d}\tau\, g^*(\omega)\left[\left(\mathcal{R}_k^{(1)} - i\frac{\tau}{2}R_k^{(1)}\right)e^{\tilde{s}_k^{(1)}\tau}e^{i\omega x_1/v}e^{i(\omega-\omega_1)\tau} + \left(\mathcal{R}_k^{(2)} + i\frac{\tau}{2}R_k^{(2)}\right)e^{\tilde{s}_k^{(2)}\tau}e^{i\omega x_2/v}e^{i(\omega-\omega_2)\tau}\right]. \tag{C13b}$$

Now, for the required overlap integrals, we need to evaluate

$$\langle\Psi_{\delta,\eta}(t)\,|\,\partial_\delta\Psi_{\delta,\eta}(t)\rangle_\delta = \sum_{m=1,2} c_m^*(t)\partial_\delta c_m(t) + \int_0^\infty \mathrm{d}\omega\,[c_R^*(\omega,t)\,\partial_\delta c_R(\omega,t) + c_L^*(\omega,t)\,\partial_\delta c_L(\omega,t)], \tag{C14a}$$

$$\langle\partial_\delta\Psi_{\delta,\eta}(t)\,|\,\partial_\delta\Psi_{\delta,\eta}(t)\rangle = \sum_{m=1,2} \partial_\delta c_m^*(t)\partial_\delta c_m(t) + \int_0^\infty \mathrm{d}\omega\,[\partial_\delta c_R^*(\omega,t)\cdot\partial_\delta c_R(\omega,t) + \partial_\delta c_L^*(\omega,t)\cdot\partial_\delta c_L(\omega,t)]. \tag{C14b}$$

In the evaluation of these overlaps, we will encounter exponential integrals of the general form, $\int_{\tau_2}^{\tau_1} dt\, t^n \exp(-\alpha t)$ over a finite domain—For the sake of brevity, we adopt the following shorthand notation in the following subsections:

$$\mathcal{G}_1(u;\tau) = \frac{e^{u\tau}}{u}, \quad \mathcal{G}_2(u;\tau) = \frac{e^{u\tau}(u\tau - 1)}{u^2}, \quad \mathcal{G}_3(u;\tau) = \frac{e^{u\tau}(u^2\tau^2 - 2u\tau + 2)}{u^3}. \tag{C15}$$

We will state the results of $\int_0^\infty d\omega\, c_R^*(\omega,t)\partial_\delta c_R(\omega,t)$ and $\int_0^\infty d\omega\, \partial_\delta c_R^*(\omega,t)\partial_\delta c_R(\omega,t)$. The integrals for $c_L(\omega,t)$ can be obtained by setting $v \to -v$. We note that the integrands can be expressed in terms of the previously derived quantities as

$$c_m^*(t)\partial_\delta c_m(t) = \sum_{\boldsymbol{k}_1,\boldsymbol{k}_2} R_{\boldsymbol{k}_1}^{(m)*}\mathcal{R}_{\boldsymbol{k}_2}^{(m)} \exp\left(\left(\tilde{s}_{\boldsymbol{k}_1}^{(1)*} + \tilde{s}_{\boldsymbol{k}_2}^{(2)}\right)\tilde{t}\right), \tag{C16}$$

$$\partial_\delta c_m^*(t)\partial_\delta c_m(t) = \sum_{\boldsymbol{k}_1,\boldsymbol{k}_2} \mathcal{R}_{\boldsymbol{k}_1}^{(m)*}\mathcal{R}_{\boldsymbol{k}_2}^{(m)} \exp\left(\left(\tilde{s}_{\boldsymbol{k}_1}^{(1)*} + \tilde{s}_{\boldsymbol{k}_2}^{(2)}\right)\tilde{t}\right). \tag{C17}$$

The evaluated integrals are expressed below. We adopt the joint subscript $\boldsymbol{j} \equiv (\sigma, j)$, where $\sigma \in \{+,-\}$ and $j \in \mathbb{Z}$, as defined in Appendix A. For practical evaluation, we finitely terminate our summation $|j| \leqslant j_{\text{cut}} = 250$:

$$\begin{aligned}
\int_0^\infty \mathrm{d}\omega\, c_R^*(\omega,t)\partial_\delta c_R(\omega,t) = {}& \frac{\gamma}{2}\sum_{\boldsymbol{k}_1,\boldsymbol{k}_2} R_{\boldsymbol{k}_1}^{(1)*}\mathcal{R}_{\boldsymbol{k}_2}^{(1)}\left[\mathcal{G}_1\left(\tilde{s}_{\boldsymbol{k}_1}^{(1)*}\tau + \tilde{s}_{\boldsymbol{k}_2}^{(1)},\tau\right)\right]_0^t - \frac{iR_{\boldsymbol{k}_1}^{(1)*}R_{\boldsymbol{k}_2}^{(1)}}{2}\left[\mathcal{G}_2\left(\tilde{s}_{\boldsymbol{k}_1}^{(1)*}\tau + \tilde{s}_{\boldsymbol{k}_2}^{(1)},\tau\right)\right]_0^t \\
&+ R_{\boldsymbol{k}_1}^{(2)*}\mathcal{R}_{\boldsymbol{k}_2}^{(2)}\left[\mathcal{G}_1\left(\tilde{s}_{\boldsymbol{k}_1}^{(2)}\tau + \tilde{s}_{\boldsymbol{k}_2}^{(2)},\tau\right)\right]_0^t + \frac{iR_{\boldsymbol{k}_1}^{(2)*}R_{\boldsymbol{k}_2}^{(2)}}{2}\left[\mathcal{G}_2\left(\tilde{s}_{\boldsymbol{k}_1}^{(2)}\tau + \tilde{s}_{\boldsymbol{k}_2}^{(2)},\tau\right)\right]_0^t \\
&+ R_{\boldsymbol{k}_1}^{(1)*}\left[\mathcal{R}_{\boldsymbol{k}_2}^{(2)} + \frac{id}{2v}R_{\boldsymbol{k}_2}^{(2)}\right]e^{+\tilde{s}_{\boldsymbol{k}_2}^{(2)}d/v - i\omega_2 d/v}\left[\mathcal{G}_1\left(\tilde{s}_{\boldsymbol{k}_1}^{(1)*} + \tilde{s}_{\boldsymbol{k}_2}^{(2)} + i\Delta\omega,\tau\right)\right]_0^{t-d/v} \\
&+ \frac{i}{2}R_{\boldsymbol{k}_1}^{(1)*}R_{\boldsymbol{k}_2}^{(2)}e^{+\tilde{s}_{\boldsymbol{k}_2}^{(2)}d/v - i\omega_2 d/v}\left[\mathcal{G}_2\left(\tilde{s}_{\boldsymbol{k}_1}^{(1)*} + \tilde{s}_{\boldsymbol{k}_2}^{(2)} + i\Delta\omega,\tau\right)\right]_0^{t-d/v} \\
&+ R_{\boldsymbol{k}_1}^{(2)*}\left[\mathcal{R}_{\boldsymbol{k}_2}^{(1)} + \frac{id}{2v}R_{\boldsymbol{k}_2}^{(1)}\right]e^{-\tilde{s}_{\boldsymbol{k}_2}^{(1)}d/v + i\omega_1 d/v}\left[\mathcal{G}_1\left(\tilde{s}_{\boldsymbol{k}_1}^{(2)} + \tilde{s}_{\boldsymbol{k}_2}^{(1)} - i\Delta\omega,\tau\right)\right]_{d/v}^t \\
&- \frac{i}{2}R_{\boldsymbol{k}_1}^{(2)*}R_{\boldsymbol{k}_2}^{(1)}e^{-\tilde{s}_{\boldsymbol{k}_2}^{(1)}d/v + i\omega_1 d/v}\left[\mathcal{G}_2\left(\tilde{s}_{\boldsymbol{k}_1}^{(2)} + \tilde{s}_{\boldsymbol{k}_2}^{(1)} - i\Delta\omega,\tau\right)\right]_{d/v}^t.
\end{aligned} \tag{C18}$$

Similarly, we evaluate $\int_0^\infty d\omega\, \partial_\delta c_R^*(\omega,t)\partial_\delta c_R(\omega,t)$ to obtain

$$\begin{aligned}
&\int_0^\infty \mathrm{d}\omega\, \partial_\delta c_R^*(\omega,t)\partial_\delta c_R(\omega,t) \\
&= \frac{\gamma}{2}\sum_{\boldsymbol{k}_1,\boldsymbol{k}_2} \mathcal{R}_{\boldsymbol{k}_1}^{(1)*}\mathcal{R}_{\boldsymbol{k}_2}^{(1)} \times \left[\mathcal{G}_1\left(\tilde{s}_{\boldsymbol{k}_1}^{(1)*} + \tilde{s}_{\boldsymbol{k}_2}^{(1)};\ \tau\right)\right]_0^t + \frac{i}{2}\left(R_{\boldsymbol{k}_1}^{(1)*}\mathcal{R}_{\boldsymbol{k}_2}^{(1)} - \mathcal{R}_{\boldsymbol{k}_1}^{(1)*}R_{\boldsymbol{k}_2}^{(1)}\right) \times \left[\mathcal{G}_2\left(\tilde{s}_{\boldsymbol{k}_1}^{(1)*} + \tilde{s}_{\boldsymbol{k}_2}^{(1)};\ \tau\right)\right]_0^t \\
&\quad + \frac{R_{\boldsymbol{k}_1}^{(1)*}R_{\boldsymbol{k}_2}^{(1)}}{4}\left[\mathcal{G}_3\left(\tilde{s}_{\boldsymbol{k}_1}^{(1)*} + \tilde{s}_{\boldsymbol{k}_2}^{(1)};\ \tau\right)\right]_0^t + \mathcal{R}_{\boldsymbol{k}_1}^{(2)*}\mathcal{R}_{\boldsymbol{k}_2}^{(2)} \times \left[\mathcal{G}_1\left(\tilde{s}_{\boldsymbol{k}_1}^{(2)} + \tilde{s}_{\boldsymbol{k}_2}^{(2)};\ \tau\right)\right]_0^t \\
&\quad + \frac{i}{2}\left(R_{\boldsymbol{k}_1}^{(2)*}\mathcal{R}_{\boldsymbol{k}_2}^{(2)} - \mathcal{R}_{\boldsymbol{k}_1}^{(2)*}R_{\boldsymbol{k}_2}^{(2)}\right) \times \left[\mathcal{G}_2\left(\tilde{s}_{\boldsymbol{k}_1}^{(2)} + \tilde{s}_{\boldsymbol{k}_2}^{(2)};\ \tau\right)\right]_0^t + \frac{R_{\boldsymbol{k}_1}^{(2)*}R_{\boldsymbol{k}_2}^{(2)}}{4}\left[\mathcal{G}_3\left(\tilde{s}_{\boldsymbol{k}_1}^{(2)} + \tilde{s}_{\boldsymbol{k}_2}^{(2)};\ \tau\right)\right]_0^t \\
&\quad + \mathcal{R}_{\boldsymbol{k}_1}^{(1)*}\left[\mathcal{R}_{\boldsymbol{k}_2}^{(2)} + \frac{id}{2v}R_{\boldsymbol{k}_2}^{(2)}\right]e^{(\tilde{s}_{\boldsymbol{k}_2}^{(2)} - i\omega_2)d/v} \times \left[\mathcal{G}_1\left(\tilde{s}_{\boldsymbol{k}_1}^{(1)*} + \tilde{s}_{\boldsymbol{k}_2}^{(2)} + i\Delta\omega;\ \tau\right)\right]_0^{t-d/v} \\
&\quad + \frac{i}{2}\left(R_{\boldsymbol{k}_1}^{(1)*}\mathcal{R}_{\boldsymbol{k}_2}^{(2)} + \mathcal{R}_{\boldsymbol{k}_1}^{(1)*}R_{\boldsymbol{k}_2}^{(2)}\right)e^{(\tilde{s}_{\boldsymbol{k}_2}^{(2)} - i\omega_2)d/v} \times \left[\mathcal{G}_2\left(\tilde{s}_{\boldsymbol{k}_1}^{(1)*} + \tilde{s}_{\boldsymbol{k}_2}^{(2)} + i\Delta\omega;\ \tau\right)\right]_0^{t-d/v} \\
&\quad - \frac{1}{4}R_{\boldsymbol{k}_1}^{(1)*}R_{\boldsymbol{k}_2}^{(2)}e^{(\tilde{s}_{\boldsymbol{k}_2}^{(2)} - i\omega_2)d/v} \times \left[\mathcal{G}_3\left(\tilde{s}_{\boldsymbol{k}_1}^{(1)*} + \tilde{s}_{\boldsymbol{k}_2}^{(2)} + i\Delta\omega;\ \tau\right)\right]_0^{t-d/v} \\
&\quad + \mathcal{R}_{\boldsymbol{k}_1}^{(2)*}\left[\mathcal{R}_{\boldsymbol{k}_2}^{(1)} + \frac{id}{2v}R_{\boldsymbol{k}_2}^{(1)}\right]e^{-(\tilde{s}_{\boldsymbol{k}_2}^{(1)} - i\omega_1)d/v} \times \left[\mathcal{G}_1\left(\tilde{s}_{\boldsymbol{k}_1}^{(2)} + \tilde{s}_{\boldsymbol{k}_2}^{(1)} - i\Delta\omega;\ \tau\right)\right]_{d/v}^t \\
&\quad - \frac{i}{2}\left(R_{\boldsymbol{k}_1}^{(2)*}\mathcal{R}_{\boldsymbol{k}_2}^{(1)} + \mathcal{R}_{\boldsymbol{k}_1}^{(2)*}R_{\boldsymbol{k}_2}^{(1)}\right)e^{-(\tilde{s}_{\boldsymbol{k}_2}^{(1)} - i\omega_1)d/v} \times \left[\mathcal{G}_2\left(\tilde{s}_{\boldsymbol{k}_1}^{(2)} + \tilde{s}_{\boldsymbol{k}_2}^{(1)} - i\Delta\omega;\ \tau\right)\right]_{d/v}^t \\
&\quad - \frac{1}{4}R_{\boldsymbol{k}_1}^{(2)*}R_{\boldsymbol{k}_2}^{(1)}e^{-(\tilde{s}_{\boldsymbol{k}_2}^{(1)} - i\omega_1)d/v} \times \left[\mathcal{G}_3\left(\tilde{s}_{\boldsymbol{k}_1}^{(2)} + \tilde{s}_{\boldsymbol{k}_2}^{(1)} - i\Delta\omega;\ \tau\right)\right]_{d/v}^t.
\end{aligned} \tag{C19}$$

Note that in the normalized time variable $\tilde{t}$, all limits are replaced by their normalized versions, i.e., $d/v \equiv \eta$ and $t - d/v \equiv \tilde{t} - \eta$. Additionally, since the overlap integrals involve double time integrals, QFI expressed in normalized time differs from the standard time variable expression by a factor of γ^2, i.e.,

$$H(\delta;\tilde{t}) = \gamma^2 H(\delta;t). \tag{C20}$$

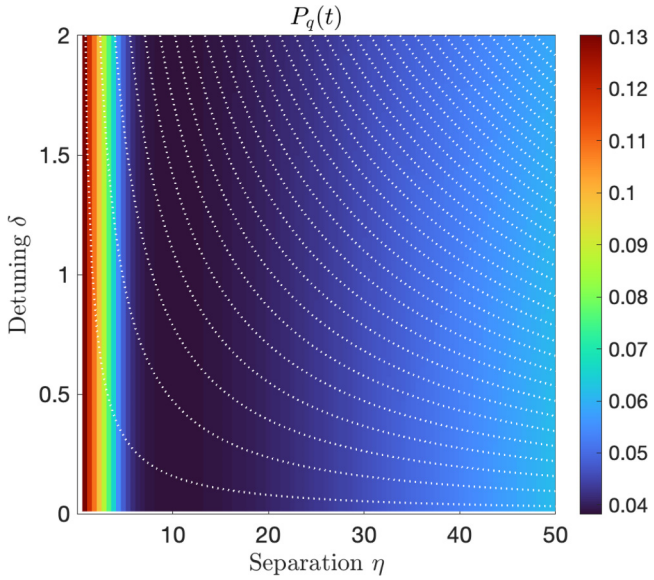


FIG. 8. Quasibound-state population P_q for $\gamma t = 1.01\eta$.

APPENDIX D: ATOM-PHOTON QUASIBOUND STATE FORMATION

In this Appendix, we expand on the steps to obtain the interatomic loss rate linked to the formation of a quasibound state in the continuum from the main text. The total probability of the single excitation being in either of the two atoms or in the field between the two atoms at any given time is

$$P_q(t) = \sum_{m=1,2} |c_m(t)|^2 + \int_{-d/2}^{d/2} \mathrm{d}x\, [|c_R(x,t)|^2 + |c_L(x,t)|^2], \tag{D1}$$

where $c_R(x,t) = \frac{1}{2\pi}\int_0^\infty \mathrm{d}\omega\, c_R(\omega,t)e^{-i\omega(t-x/v)}$ and $c_L(x,t) = \frac{1}{2\pi}\int_0^\infty \mathrm{d}\omega\, c_L(\omega,t)e^{-i\omega(t+x/v)}$ are the inverse Fourier transforms of $c_R(\omega,t)$ and $c_L(\omega,t)$. We wish to compute the rate at which this excitation probability changes over time:

$$\frac{\mathrm{d}P_q(t)}{\mathrm{d}t} = 2\mathrm{Re}\left\{\sum_{m=1,2} \dot{c}_m^*(t)c_m(t) + \int_{-d/2}^{d/2} \mathrm{d}x\, [\dot{c}_R^*(x,t)c_R(x,t) + \dot{c}_L^*(x,t)c_L(x,t)]\right\} \equiv \Gamma(t). \tag{D2}$$

The values of η and δ that locally minimize $\Gamma(t)$ correspond to a slow excitation loss from the effective cavity formed by the two atoms, indicating the formation of a qBIC (as depicted in Fig. 8). The transformation of the field amplitudes from frequency to position domain gives us

$$c_R(x,t) = -\frac{i}{2\pi}\int_0^\infty \mathrm{d}\omega g^*(\omega)\int_0^t \mathrm{d}\tau\, [c_1(\tau)e^{i\omega d/2v}e^{i(\omega-\omega_1)\tau} + c_2(\tau)e^{-i\omega d/2v}e^{i(\omega-\omega_2)\tau}]e^{-i\omega(t-x/v)}, \tag{D3}$$

$$c_L(x,t) = -\frac{i}{2\pi}\int_0^\infty \mathrm{d}\omega g^*(\omega)\int_0^t \mathrm{d}\tau\, [c_1(\tau)e^{-i\omega d/2v}e^{i(\omega-\omega_1)\tau} + c_2(\tau)e^{i\omega d/2v}e^{i(\omega-\omega_2)\tau}]e^{-i\omega(t+x/v)}. \tag{D4}$$

Again, assuming a flat-spectral density of the waveguide [i.e., $g(\omega) = g(\omega_0)$] and simplifying the integrals gives us the spatial domain field expressions,

$$\begin{aligned} c_R(x,t) = -\frac{ig^*(\omega_0)}{2}\{&c_1(t-(x-d/2)/v)e^{-i\omega_1(t-(x-d/2)/v)}[\Theta(t-(x-d/2)/v) - \Theta(-(x-d/2)/v)] \\ &+ c_2(t-(x+d/2)/v)e^{-i\omega_2(t-(x+d/2)/v)}[\Theta(t-(x+d/2)/v) - \Theta(-(x+d/2)/v)]\}, \end{aligned} \tag{D5a}$$

$$\begin{aligned} c_L(x,t) = -\frac{ig^*(\omega_0)}{2}\{&c_1(t+(x+d/2)/v)e^{-i\omega_1(t+(x+d/2)/v)}[\Theta(t+(x+d/2)/v) - \Theta((x+d/2)/v)] \\ &+ c_2(t+(x-d/2)/v)e^{-i\omega_2(t+(x-d/2)/v)}[\Theta(t+(x-d/2)/v) - \Theta((x-d/2)/v)]\}. \end{aligned} \tag{D5b}$$

In Eq. (D5a), the $c_1(\cdot)$ term gives rise to fields emanated to the right from the atom at x_1 and the $c_2(\cdot)$ term gives rise to fields emanated to the right from the atom at x_2. Correspondingly, in Eq. (D5b), these terms are fields emanating to the left from each atom. Consequently, we note that the second line of Eq. (D5a) and first line of Eq. (D5b) fall outside the region $x \in [-d/2, d/2]$,

resulting in terms in the expansion of $|c_{\{a,b\}}(x,t)|^2$ that do not contribute to the integral of Eq. (D1), allowing us to simplify as

$$\int_{-d/2}^{d/2} \mathrm{d}x\,[|c_R(x,t)|^2+|c_L(x,t)|^2] = \frac{\gamma}{8\pi}\int_{-d/2}^{d/2}\mathrm{d}x\,\{|c_1(t-(x-d/2)/v)|^2[\Theta(t-(x-d/2)/v)-\Theta(-(x-d/2)/v)] + |c_2(t+(x-d/2)/v)|^2[\Theta(t+(x-d/2)/v)-\Theta((x-d/2)/v)]\} \equiv \mathcal{I}. \tag{D6}$$

The constraints imposed by the step function in the above expressions lead to two different results for times $0 \leqslant t \leqslant d/v$ (radiation has not yet reached the second atom) and $t > d/v$ (radiation has reached the second atom and some is lost). Thus, the integral gets its limits rearranged as follows:

$$\mathcal{I} = \begin{cases} \frac{\gamma}{8\pi}\left[\int_{-d/2}^{vt-d/2}\mathrm{d}x\,|c_1(t-(x-d/2)/v)|^2 + \int_{d/2-vt}^{d/2}\mathrm{d}x\,|c_2(t+(x-d/2)/v)|^2\right], & t\in[0,d/v), \\ \frac{\gamma}{8\pi}\int_{-d/2}^{d/2}\mathrm{d}x[|c_1(t-(x-d/2)/v)|^2 + |c_2(t+(x-d/2)/v)|^2], & t > d/v. \end{cases} \tag{D7}$$

We simplify these integrals by substituting the atomic coefficients in their expanded forms

$$c_m(t) \equiv \sum_j^{\infty} R_j^{(m)} e^{s_j^{(m)}t}. \tag{D8}$$

The following simplified expressions are evaluated by taking the necessary definite spatial integrals:

$$\mathcal{I}(0\leqslant t\leqslant d/v) = \frac{\gamma}{8\pi}\sum_{j,k}\left[-R_j^{(1)}R_k^{*(1)}\Big/\left\{s_j^{(1)}+s_k^{(1)*}\right\} + R_j^{(1)}R_k^{*(1)}\exp\left(\left\{s_j^{(1)}+s_k^{(1)*}\right\}t\right)\Big/\left\{s_j^{(1)}+s_k^{(1)*}\right\} + R_j^{(2)}R_k^{*(2)}\exp\left(\left\{s_j^{(2)}+s_k^{(2)*}\right\}\tilde{t}\right)\Big/\left\{s_j^{(2)}+s_k^{(2)*}\right\} - R_j^{(2)}R_k^{*(2)}\Big/\left\{s_j^{(2)}+s_k^{(2)*}\right\}\right], \tag{D9}$$

$$\mathcal{I}(t>d/v) = \frac{\gamma}{8\pi}\sum_{j,k}\left[-\left\{R_j^{(1)}R_k^{*(1)}\exp\left(\left\{s_j^{(1)}+s_k^{(1)*}\right\}\{t-d/v\}\right) - R_j^{(1)}R_k^{*(1)}\exp\left(\left\{s_j^{(1)}+s_k^{(1)*}\right\}t\right)\right\}\Big/\left\{s_j^{(1)}+s_k^{(1)*}\right\} + \left\{R_j^{(2)}R_k^{*(2)}\exp\left(\left\{s_j^{(2)}+s_k^{(2)*}\right\}t\right) - R_j^{(2)}R_k^{*(2)}\exp\left(\left\{s_j^{(2)}+s_k^{(2)*}\right\}\{t-d/v\}\right)\right\}\Big/\left\{s_j^{(2)}+s_k^{(2)*}\right\}\right]. \tag{D10}$$

These equations [Eqs. (D9) and (D10)] represent the probability of the single excitation being in the field modes between the two atoms. Now, we can calculate the loss rate from the field modes by taking the time derivative:

$$\dot{I}_1(0\leqslant t\leqslant d/v) = \frac{\gamma}{8\pi}\sum_{j,k}\left[R_j^{(1)}R_k^{*(1)}\exp\left(\left\{s_j^{(1)}+s_k^{(1)*}\right\}t\right) + R_j^{(2)}R_k^{*(2)}\exp\left(\left\{s_j^{(2)}+s_k^{(2)*}\right\}t\right)\right] = \frac{\gamma}{8\pi}[|c_1(t)|^2+|c_2(t)|^2], \tag{D11}$$

$$\dot{I}_2(t>d/v) = \frac{\gamma}{8\pi}\sum_{j,k}\left[-R_j^{(1)}R_k^{*(1)}\exp\left(\left\{s_j^{(1)}+s_k^{(1)*}\right\}\{t-d/v\}\right) + R_j^{(1)}R_k^{*(1)}\exp\left(\left\{s_j^{(1)}+s_k^{(1)*}\right\}t\right) + R_j^{(2)}R_k^{*(2)}\exp\left(\left\{s_j^{(2)}+s_k^{(2)*}\right\}t\right) - R_j^{(2)}R_k^{*(2)}\exp\left(\left\{s_j^{(2)}+s_k^{(2)*}\right\}\{t-d/v\}\right)\right] = \frac{\gamma}{8\pi}[-|c_1(t-d/v)|^2+|c_1(t)|^2+|c_2(t)|^2-|c_2(t-d/v)|^2]. \tag{D12}$$

On the other hand, the loss rate of the atoms is given as $\Gamma_{\text{atoms}} = \partial_t[|c_1(t)|^2+|c_2(t)|^2] = 2\mathrm{Re}[\dot{c}_1(t)c_1^*(t)+\dot{c}_2(t)c_2^*(t)]$. Combining these results for field and atomic loss rates, we have

$$\Gamma(t) = \begin{cases} \sum_{m=1,2}\left[2\ \mathrm{Re}(\dot{c}_m^*(t)c_m(t)) + \frac{\gamma}{8\pi}|c_m(t)|^2\right], & 0\leqslant t\leqslant d/v, \\ \sum_{m=1,2}\left[2\ \mathrm{Re}(\dot{c}_m^*(t)c_m(t)) + \frac{\gamma}{8\pi}(|c_m(t)|^2-|c_m(t-d/v)|^2)\right], & t>d/v, \end{cases} \tag{D13}$$

where the second line corresponds to Eq. (35). In order to determine qBIC conditions, we minimize the loss rate Γ with respect to the detuning δ. As we care about late-time dynamics, we only minimize the expression for $t > d/v$. By substituting the expressions for the atomic dynamics, the extrema are found from the equation $\partial_\delta\Gamma(t>d/v)=0$.

APPENDIX E: QUANTUM FISHER INFORMATION FOR NONINTERACTING EMITTERS

We analyze a reference scenario consisting of two identical noninteracting emitters, each coupled to an independent waveguide. Considering the initial state, $|\Psi(t=0)\rangle = \sigma_+^{(m)}|g,g,\{0\}_1,\{0\}_2\rangle$, where $|\{0\}_m\rangle$ represents the waveguide modes coupled to the mth emitter, Wigner-Weisskopf theory gives us the joint state

$$|\Psi(t)\rangle = e^{-(\gamma/2+i\omega_m)t}\sigma_+^{(m)}|g,g\rangle\otimes|\{0\}_1,\{0\}_2\rangle + |g,g\rangle\otimes\int_0^t \mathrm{d}\tau\,\xi(\tau)[a_m^\dagger(\tau)+b_m^\dagger(\tau)]\,|\{0\}_1,\{0\}_2\rangle, \tag{E1}$$

where $a_m^\dagger(t')$, $b_m^\dagger(t')$ are creation operations corresponding to left- and right-going temporal modes for the waveguide coupled to emitter m. The photon temporal wave packet is given by $\xi(t') = \sqrt{\frac{\gamma}{2}} e^{-(\gamma/2+i\omega_m)t'}$, where ω_m is the center frequency and γ is the overall atomic coupling rate to the waveguide. To evaluate the QFI, we calculate

$$\left|\partial_{\omega_m}\Psi(t)\right\rangle = -ite^{-(\gamma/2+i\omega_m)t}\sigma_+^{(m)}|g,g\rangle \otimes |\{0\}_1,\{0\}_2\rangle - |g,g\rangle \otimes \int_0^t d\tau\, i\tau\xi(\tau)[a_m^\dagger(\tau)+b_m^\dagger(\tau)]\,|\{0\}_1,\{0\}_2\rangle. \tag{E2}$$

Evaluating the QFI $H(\omega_m) = 4(\mathrm{Re}\langle\partial_{\omega_m}\Psi(t)|\partial_{\omega_m}\Psi(t)\rangle + \langle\Psi(t)|\partial_{\omega_m}\Psi(t)\rangle^2)$, we get

$$\begin{aligned}\left\langle\partial_{\omega_m}\Psi(t)\right\rangle &= t^2e^{-\gamma t} + 2\int_0^t d\tau \int_0^t d\tau'\,\tau\tau'\xi(\tau)\xi(\tau')\delta(\tau-\tau') = t^2e^{-\gamma t} + \gamma\int_0^t d\tau\,\tau^2e^{-\gamma\tau} \\ &= t^2e^{-\gamma t} + \frac{2-e^{-\gamma t}(2+2\gamma t+\gamma^2t^2)}{\gamma^2} = \frac{2(1-e^{-\gamma t}-\gamma te^{-\gamma t})}{\gamma^2},\end{aligned} \tag{E3}$$

$$\begin{aligned}\left\langle\Psi(t)\middle|\partial_{\omega_m}\Psi(t)\right\rangle &= -ite^{-\gamma t} - 2i\int_0^t d\tau \int_0^t d\tau'\,\tau'\xi(\tau)\xi(\tau')\delta(\tau-\tau') = -ite^{-\gamma t} - i\gamma\int_0^t d\tau\;\tau e^{-\gamma\tau} \\ &= -ite^{-\gamma t} - i\frac{1-e^{-\gamma t}(1+\gamma t)}{\gamma} = -i\frac{1-e^{-\gamma t}}{\gamma},\end{aligned} \tag{E4}$$

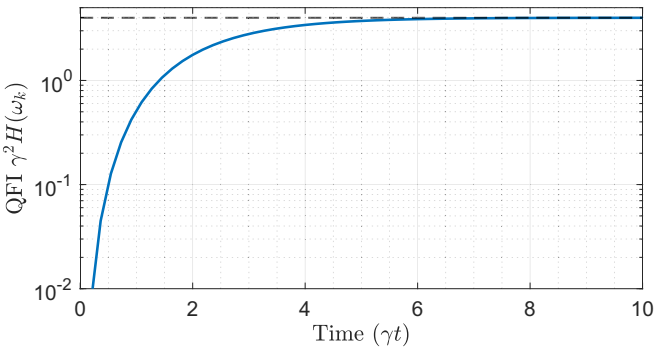


FIG. 9. Plot of QFI $\gamma^2 H(\omega_m)$ for noninteracting emitters as a function of time.

which gives us $H(\omega_m) = 4(1-(e^{-\gamma t}+2\gamma t)e^{-\gamma t})/\gamma^2$ (see plot in Fig. 9). It is important to note that the QFI is only determined by the coupling rate to the waveguide modes. In fact, if the waveguide modes are traced out, we have the state

$$\rho_{E_i} = e^{-\gamma t}|e\rangle\langle e|_i + (1-e^{-\gamma t})|g\rangle\langle g|_i. \tag{E5}$$

Since the state has no dependence on ω_i, we have $\partial_{\omega_i}\rho_{E_i} = 0$, which consequently implies that the QFI is zero when the field modes are traced out.

We use the expression for the QFI of a parameter, $H(\theta) = H(f(\theta)) \times (\frac{df(\theta)}{d\theta})^2$, to obtain the normalized frequency units QFI as $\lim_{t\to\infty} H(\tilde{\omega}_m) = \gamma^2 \lim_{t\to\infty} H(\omega_m) = 4$.

[1] H. J. Kimble, The quantum internet, Nature (London) **453**, 1023 (2008).

[2] A. Sipahigil, R. E. Evans, D. D. Sukachev, M. J. Burek, J. Borregaard, M. K. Bhaskar, C. T. Nguyen, J. L. Pacheco, H. A. Atikian, C. Meuwly, R. M. Camacho, F. Jelezko, E. Bielejec, H. Park, M. Lončar, and M. D. Lukin, An integrated diamond nanophotonics platform for quantum-optical networks, Science **354**, 847 (2016).

[3] A. Javadi, I. Söllner, M. Arcari, S. L. Hansen, L. Midolo, S. Mahmoodian, G. Kiršanskė, T. Pregnolato, E. H. Lee, J. D. Song, S. Stobbe, and P. Lodahl, Single-photon non-linear optics with a quantum dot in a waveguide, Nat. Commun. **6**, 8655 (2015).

[4] S. Faez, P. Türschmann, H. R. Haakh, S. Götzinger, and V. Sandoghdar, Coherent interaction of light and single molecules in a dielectric nanoguide, Phys. Rev. Lett. **113**, 213601 (2014).

[5] A. Laucht, S. Pütz, T. Günthner, N. Hauke, R. Saive, S. Frédérick, M. Bichler, M.-C. Amann, A. W. Holleitner, M. Kaniber, and J. J. Finley, A waveguide-coupled on-chip single-photon source, Phys. Rev. X **2**, 011014 (2012).

[6] A. Asenjo-Garcia, M. Moreno-Cardoner, A. Albrecht, H. J. Kimble, and D. E. Chang, Exponential improvement in photon storage fidelities using subradiance and "selective radiance" in atomic arrays, Phys. Rev. X **7**, 031024 (2017).

[7] C. Sayrin, C. Junge, R. Mitsch, B. Albrecht, D. O'Shea, P. Schneeweiss, J. Volz, and A. Rauschenbeutel, Nanophotonic optical isolator controlled by the internal state of cold atoms, Phys. Rev. X **5**, 041036 (2015).

[8] W. Konyk and J. Gea-Banacloche, Passive, deterministic photonic conditional-phase gate via two-level systems, Phys. Rev. A **99**, 010301 (2019).

[9] N. V. Corzo, J. Raskop, A. Chandra, A. S. Sheremet, B. Gouraud, and J. Laurat, Waveguide-coupled single collective excitation of atomic arrays, Nature (London) **566**, 359 (2019).

[10] G. Angelatos and S. Hughes, Entanglement dynamics and Mollow nonuplets between two coupled quantum dots in a nanowire photonic-crystal system, Phys. Rev. A **91**, 051803 (2015).

[11] K. Sinha, P. Meystre, E. A. Goldschmidt, F. K. Fatemi, S. L. Rolston, and P. Solano, Non-Markovian collective emission

from macroscopically separated emitters, Phys. Rev. Lett. **124**, 043603 (2020).

[12] F. Dinc and A. M. Brańczyk, Non-Markovian super-superradiance in a linear chain of up to 100 qubits, Phys. Rev. Res. **1**, 032042 (2019).

[13] F. Dinc, İ. Ercan, and A. M. Brańczyk, Exact Markovian and non-Markovian time dynamics in waveguide QED: Collective interactions, bound states in continuum, superradiance and subradiance, Quantum **3**, 213 (2019).

[14] G. Calajó, Y.-L. L. Fang, H. U. Baranger, and F. Ciccarello, Exciting a bound state in the continuum through multiphoton scattering plus delayed quantum feedback, Phys. Rev. Lett. **122**, 073601 (2019).

[15] P. Facchi, D. Lonigro, S. Pascazio, F. V. Pepe, and D. Pomarico, Bound states in the continuum for an array of quantum emitters, Phys. Rev. A **100**, 023834 (2019).

[16] K. Sinha, P. Meystre, and P. Solano, Non-Markovian dynamics of collective atomic states coupled to a waveguide, in *Quantum Nanophotonic Materials, Devices, and Systems 2019*, edited by C. Soci, M. T. Sheldon, and M. Agio, Society for Optics and Photonics Vol. 11091 (SPIE, 2019), p. 110910O.

[17] A. Carmele, N. Nemet, V. Canela, and S. Parkins, Pronounced non-Markovian features in multiply excited, multiple emitter waveguide QED: Retardation induced anomalous population trapping, Phys. Rev. Res. **2**, 013238 (2020).

[18] K. Barkemeyer, A. Knorr, and A. Carmele, Strongly entangled system-reservoir dynamics with multiphoton pulses beyond the two-excitation limit: Exciting the atom-photon bound state, Phys. Rev. A **103**, 033704 (2021).

[19] R. Trivedi, D. Malz, S. Sun, S. Fan, and J. Vučković, Optimal two-photon excitation of bound states in non-Markovian waveguide QED, Phys. Rev. A **104**, 013705 (2021).

[20] G. Magnifico, M. Maffei, D. Pomarico, D. Das, P. Facchi, S. Pascazio, and F. V. Pepe, Non-Markovian dynamics of generation of bound states in the continuum via single-photon scattering, Phys. Rev. Res. **7**, 033249 (2025).

[21] K. Sinha, A. González-Tudela, Y. Lu, and P. Solano, Collective radiation from distant emitters, Phys. Rev. A **102**, 043718 (2020).

[22] S. Arranz Regidor and S. Hughes, Cavitylike strong coupling in macroscopic waveguide QED using three coupled qubits in the deep non-Markovian regime, Phys. Rev. A **104**, L031701 (2021).

[23] D. Cilluffo, L. Ferialdi, G. M. Palma, G. Calajò, and F. Ciccarello, Multimode-cavity picture of non-Markovian waveguide QED, Phys. Rev. Res. **8**, 023172 (2026).

[24] A. Das, P. Solano, and K. Sinha, Non-Markovian spontaneous emission in a tunable cavity formed by atomic mirrors, Phys. Rev. A **112**, 043723 (2025).

[25] A. Keefe, N. Agarwal, and A. Kamal, Quantifying spectral signatures of non-Markovianity beyond the Born-Redfield master equation, Quantum **9**, 1863 (2025).

[26] H. Pichler, S. Choi, P. Zoller, and M. D. Lukin, Universal photonic quantum computation via time-delayed feedback, Proc. Natl. Acad. Sci. USA **114**, 11362 (2017).

[27] H. Pichler and P. Zoller, Photonic circuits with time delays and quantum feedback, Phys. Rev. Lett. **116**, 093601 (2016).

[28] W. Alvarez-Giron, P. Solano, K. Sinha, and P. Barberis-Blostein, Delay-induced spontaneous dark-state generation from two distant excited atoms, Phys. Rev. Res. **6**, 023213 (2024).

[29] H. Zheng and H. U. Baranger, Persistent quantum beats and long-distance entanglement from waveguide-mediated interactions, Phys. Rev. Lett. **110**, 113601 (2013).

[30] R. L. Capurso, G. Calajó, S. Montangero, *et al.*, Superradiant decay in non-Markovian waveguide quantum electrodynamics, Commun. Phys. **9**, 342 (2026).

[31] G. Crowder, L. Ramunno, and S. Hughes, Improving on-demand single-photon-source coherence and indistinguishability through a time-delayed coherent feedback, Phys. Rev. A **110**, L031703 (2024).

[32] A. L. Grimsmo, Time-delayed quantum feedback control, Phys. Rev. Lett. **115**, 060402 (2015).

[33] H.-P. Breuer, E.-M. Laine, J. Piilo, and B. Vacchini, *Colloquium*: Non-Markovian dynamics in open quantum systems, Rev. Mod. Phys. **88**, 021002 (2016).

[34] I. de Vega and D. Alonso, Dynamics of non-Markovian open quantum systems, Rev. Mod. Phys. **89**, 015001 (2017).

[35] C. W. Helstrom, Quantum detection and estimation theory, J. Stat. Phys. **1**, 231 (1969).

[36] G. Tóth and I. Apellaniz, Quantum metrology from a quantum information science perspective, J. Phys. A: Math. Theor. **47**, 424006 (2014).

[37] J. F. Barry, J. M. Schloss, E. Bauch, M. J. Turner, C. A. Hart, L. M. Pham, and R. L. Walsworth, Sensitivity optimization for NV-diamond magnetometry, Rev. Mod. Phys. **92**, 015004 (2020).

[38] D. Schäffner, T. Schreiber, F. Lenz, M. Schlosser, and G. Birkl, Quantum sensing in tweezer arrays: Optical magnetometry on an individual-atom sensor grid, PRX Quantum **5**, 010311 (2024).

[39] W. Muessel, H. Strobel, D. Linnemann, D. B. Hume, and M. K. Oberthaler, Scalable spin squeezing for quantum-enhanced magnetometry with Bose-Einstein condensates, Phys. Rev. Lett. **113**, 103004 (2014).

[40] Y. Li, L. Joosten, Y. Baamara, P. Colciaghi, A. Sinatra, P. Treutlein, and T. Zibold, Multiparameter estimation with an array of entangled atomic sensors, Science **391**, 374 (2026).

[41] L. Pezzè, A. Smerzi, M. K. Oberthaler, R. Schmied, and P. Treutlein, Quantum metrology with nonclassical states of atomic ensembles, Rev. Mod. Phys. **90**, 035005 (2018).

[42] S. Kukita, Y. Matsuzaki, and Y. Kondo, Heisenberg-limited quantum metrology using collective dephasing, Phys. Rev. Appl. **16**, 064026 (2021).

[43] F. Belliardo, A. Chu, M. Koppenhöfer, and A. A. Clerk, Extracting information from a superradiant burst using simple measurements, PRX Quantum (2026), doi:10.1103/1m4s-kky2.

[44] A. J. Brady, Y.-X. Wang, V. V. Albert, A. V. Gorshkov, and Q. Zhuang, Correlated noise estimation with quantum sensor networks, Phys. Rev. Lett. **136**, 080803 (2026).

[45] V. Giovannetti, S. Lloyd, and L. Maccone, Quantum metrology, Phys. Rev. Lett. **96**, 010401 (2006).

[46] P. W. Milonni and P. L. Knight, Retardation in the resonant interaction of two identical atoms, Phys. Rev. A **10**, 1096 (1974).

[47] P. W. Milonni and P. L. Knight, Retarded interaction of two nonidentical atoms, Phys. Rev. A **11**, 1090 (1975).

[48] A. Lee, H. S. Han, F. K. Fatemi, S. L. Rolston, and K. Sinha, Collective quantum beats from distant multilevel emitters, Phys. Rev. A **107**, 013701 (2023).

[49] P. Meystre and M. Sargent, *Elements of Quantum Optics* (Springer, Berlin, 2007).

[50] S. L. Braunstein and C. M. Caves, Statistical distance and the geometry of quantum states, Phys. Rev. Lett. **72**, 3439 (1994).

[51] A. Fujiwara and H. Nagaoka, Quantum Fisher metric and estimation for pure state models, Phys. Lett. A **201**, 119 (1995).

[52] It is important to note that $|\partial_\delta \Psi_{\delta,\eta}(t)\rangle$ and $\langle \partial_\delta \Psi_{\delta,\eta}(t)|$ are differential unit vectors defined for the state $|\Psi(t)\rangle$ and its dual; they are not necessarily self-dual, i.e., in general, $\langle \partial_\delta \Psi(t) \,|\, \partial_\delta \Psi(t)\rangle \neq 1$.

[53] H.-N. Xiong, L. Li, Z. Sun, Z. Yang, Z. Le, Y. Huang, and X. Wang, Information preservation of two qubits in a structured environment, New J. Phys. **24**, 123001 (2022).

[54] R. Pennetta, M. Blaha, A. Johnson, D. Lechner, P. Schneeweiss, J. Volz, and A. Rauschenbeutel, Collective radiative dynamics of an ensemble of cold atoms coupled to an optical waveguide, Phys. Rev. Lett. **128**, 073601 (2022).

[55] D. Lechner, R. Pennetta, M. Blaha, P. Schneeweiss, A. Rauschenbeutel, and J. Volz, Light-matter interaction at the transition between cavity and waveguide QED, Phys. Rev. Lett. **131**, 103603 (2023).

[56] A. Lee, Collective dynamics of atoms coupled to an optical nanofiber: From disordered ensembles to tunable arrays, Ph.D. thesis, University of Maryland, College Park, 2025, digital repository at the University of Maryland (DRUM).

[57] M. Mirhosseini, E. Kim, V. S. Ferreira, M. Kalaee, A. Sipahigil, A. J. Keller, and O. Painter, Superconducting metamaterials for waveguide quantum electrodynamics, Nat. Commun. **9**, 3706 (2018).

[58] B. Kannan, M. J. Ruckriegel, D. L. Campbell, A. Frisk Kockum, J. Braumüller, D. K. Kim, M. Kjaergaard, P. Krantz, A. Melville, B. M. Niedzielski, A. Vepsäläinen, R. Winik, J. L. Yoder, F. Nori, T. P. Orlando, S. Gustavsson, and W. D. Oliver, Waveguide quantum electrodynamics with superconducting artificial giant atoms, Nature (London) **583**, 775 (2020).

[59] V. S. Ferreira, J. Banker, A. Sipahigil, M. H. Matheny, A. J. Keller, E. Kim, M. Mirhosseini, and O. Painter, Collapse and revival of an artificial atom coupled to a structured photonic reservoir, Phys. Rev. X **11**, 041043 (2021).

[60] B. Kannan, A. Almanakly, Y. Sung, A. Di Paolo, D. A. Rower, J. Braumüller, A. Melville, B. M. Niedzielski, A. Karamlou, K. Serniak, A. Vepsäläinen, M. E. Schwartz, J. L. Yoder, R. Winik, J. I.-J. Wang, T. P. Orlando, S. Gustavsson, J. A. Grover, and W. D. Oliver, On-demand directional microwave photon emission using waveguide quantum electrodynamics, Nat. Phys. **19**, 394 (2023).

[61] S. Storz, A. Kulikov, J. D. Schär, V. Barizien, X. Valcarce, F. Berterottière, N. Sangouard, J.-D. Bancal, and A. Wallraff, Complete self-testing of a system of remote superconducting qubits, Phys. Rev. Lett. **135**, 030801 (2025).

[62] C.-Y. Chen, G. Crowder, Z.-Q. Niu, P. Y. Wen, Y.-H. Lin, J.-C. Chen, Z.-R. Lin, F. Nori, S. Hughes, and I.-C. Hoi, Resonance fluorescence of an artificial atom with a time-delayed coherent feedback, arXiv:2603.28004.

[63] A. Hernández-Antón, J. D. Schär, A. Grigorev, G. F. Penas, R. Puebla, J. J. García-Ripoll, J.-C. Besse, A. Wallraff, and A. Kulikov, Emission and absorption of microwave photons in orthogonal temporal modes across a 30-meter two-node network, arXiv:2604.12947.

[64] J.-H. Kim, S. Aghaeimeibodi, C. J. K. Richardson, R. P. Leavitt, and E. Waks, Super-radiant emission from quantum dots in a nanophotonic waveguide, Nano Lett. **18**, 4734 (2018).

[65] A. Tiranov, V. Angelopoulou, C. J. van Diepen, B. Schrinski, O. A. D. Sandberg, Y. Wang, L. Midolo, S. Scholz, A. D. Wieck, A. Ludwig, A. S. Sørensen, and P. Lodahl, Collective super- and subradiant dynamics between distant optical quantum emitters, Science **379**, 389 (2023).

[66] S. Longhi, Superradiance paradox in waveguide lattices, Opt. Lett. **45**, 3297 (2020).

[67] R. A. Vicencio, F. G. L. Cárcamo-Macaya, D. Román-Cortés, and P. Solano, Observation of non-Markovian radiative phenomena in structured photonic lattices, Phys. Rev. Lett. **135**, 013601 (2025).

[68] L. Krinner, M. Stewart, A. Pazmiño, J. Kwon, and D. Schneble, Spontaneous emission of matter waves from a tunable open quantum system, Nature (London) **559**, 589 (2018).

[69] Y. Kim, A. Lanuza, and D. Schneble, Super- and subradiant dynamics of quantum emitters mediated by atomic matter waves, Nat. Phys. **21**, 70 (2025).

[70] B. Windt, M. Bello, D. Malz, and J. I. Cirac, Effects of retardation on many-body superradiance in chiral waveguide QED, Phys. Rev. Lett. **134**, 173601 (2025).

[71] C. Barahona-Pascual, H. Jiang, A. C. Santos, and J. J. García-Ripoll, Time-delayed collective dynamics in waveguide QED and bosonic quantum networks, Quantum Sci. Technol. **11**, 015016 (2026).

[72] S. Arranz Regidor, G. Crowder, H. Carmichael, and S. Hughes, Modeling quantum light-matter interactions in waveguide QED with retardation, nonlinear interactions, and a time-delayed feedback: Matrix product states versus a space-discretized waveguide model, Phys. Rev. Res. **3**, 023030 (2021).

[73] O. A. D. Sandberg, S. Ostermann, and S. F. Yelin, Cooperative sensing with impurities in a two-dimensional subwavelength array, Phys. Rev. A **111**, 032603 (2025).

[74] C. W. Hsu, B. Zhen, A. Douglas Stone, J. D. Joannopoulos, and M. Soljačić, Bound states in the continuum, Nat. Rev. Mater. **1**, 16048 (2016).

[75] U. Dorner and P. Zoller, Laser-driven atoms in half-cavities, Phys. Rev. A **66**, 023816 (2002).

[76] A. Del Ángel, P. Solano, and P. Barberis-Blostein, Effects of environment correlations on the onset of collective decay in waveguide QED, Phys. Rev. A **108**, 013703 (2023).

[77] A. González-Tudela and J. I. Cirac, Markovian and non-Markovian dynamics of quantum emitters coupled to two-dimensional structured reservoirs, Phys. Rev. A **96**, 043811 (2017).

[78] *Handbook of Mathematical Functions*, edited by M. Abramowitz and I. A. Stegun (Dover Publications, 2012).

[79] I. S. Gradshteyn and I. M. Ryzhik, *Table of Integrals, Series, and Products* (Academic Press, 2014).

[80] R. M. Corless, G. H. Gonnet, D. E. G. Hare, D. J. Jeffrey, and D. E. Knuth, On the Lambert *W* function, Adv. Comput. Math. **5**, 329 (1996).